August 1973 LMSC-D352320

UNSTEADY AERODYNAMIC ANALYSIS OF SPACE SHUTTLE VEHICLES

Part I: SUMMARY REPORT

Final Technical Report

Prepared by

Lars E. Ericsson
Consulting Engineer, Engineering Technology

J. Peter Reding
Research Specialist Aero-Thermodynamics

Prepared Under Contract NAS 8-28130
for
National Aeronautics and Space Administration

Lockheed MISSILES & SPACE COMPANY, INC.
SUNNYVALE, CALIFORNIA

UNSTEADY AERODYNAMIC ANALYSIS OF SPACE SHUTTLE VEHICLES

Part I: SUMMARY REPORT

by
Lars E. Ericsson and J. Peter Reding

August 1973

Prepared Under Contract NAS 8-28130
for
National Aeronautics and Space Administration

Lockheed Missiles & Space Company, Inc.
A Subsidiary of Lockheed Aircraft Corporation
Sunnyvale, California

ABSTRACT

An analysis of the unsteady aerodynamics of space shuttle vehicles has been performed. The results show that slender wing theory can be modified to give the potential flow static and dynamic characteristics over a large Mach number range from $M = 0$ to $M > 1$. A semi-empirical analytic approximation is derived for the loads induced by the leading edge vortex; and it is shown that the developed analytic technique gives good prediction of experimentally determined steady and unsteady delta-wing aerodynamics, including the effects of leading edge roundness. At supersonic speeds, attached leading edge flow is established and shock-induced flow separation effects become of concern. Analysis of experimental results for a variety of boost configurations has led to a definition of the main features of the flow interference effects between orbiter (delta wing) and booster. The effects of control deflection on the unsteady aerodynamics of the delta-wing orbiter have also been evaluated using available experimental data. The results indicate that the effects of delta platform lifting surfaces can be included in a simple manner when determining elastic launch vehicle dynamic characteristics.

CONTENTS

ILLUSTRATIONS

Section 1
INTRODUCTION

It was clear very early in the space shuttle development that the vehicle design could be critically dependent upon aeroelastic loads (Refs. 1 and 2). The complexity of the flow field prohibits the prediction of unsteady aerodynamic loads by purely theoretical means. Experience with the Saturn-Apollo design made clear that one cannot rely solely on dynamic experiments either, because the long lead time needed for the elastic model design in combination with the continuing changes of the flight vehicle ensures that the test results will be obsolete when finally obtained. Regardless of their accuracy, the test data are of no help unless they can be extrapolated analytically to apply to the current flight vehicle design.

NASA Marshall Space Flight Center (MSFC) needed, therefore, to develop analytic methods in time to be applicable to the final space shuttle design. Lockheed developed such analytical means for the Saturn-Apollo launch vehicles (Ref. 3), and the predictions agreed so well with the elastic wind tunnel test results for the Saturn I booster (Ref. 4) that this technique was used to predict the aeroelastic characteristics of all future Saturn boosters (Ref. 5), thus eliminating the need for further complicated elastic model tests (e.g., Ref. 6).

The success of the Saturn analysis led NASA MSFC to retain Lockheed to develop the method further to provide the needed analytic tools for the space shuttle boost configuration. The main difficulty when extending the Saturn analysis (Refs. 3 through 5) to apply to the space shuttle launch vehicle is presented by the orbiter delta wing. The work leading to the formulation of simple analytic means for predicting the unsteady aerodynamics of sharp-edged delta wings, including the effects of leading edge vortices, is reported in detail in Part II of this report (Ref. 7); these results are summarized here. The effects of leading edge roundness and Mach number on the unsteady delta-wing aerodynamics are discussed here in full detail, however, as they are not reported elsewhere. Available experimental results for a variety of boost

configurations have been analyzed to define the main features of the interference flow field imposed upon the orbiter delta wing (and fuselage) from the hydrogen-oxygen (HO) tank and solid rocket motors (SRMs), including the effects of exhaust plumes. The results are reported in detail in Part III of this report (Ref. 8) and are only summarized here. Finally, a summary is given of the control-induced effects on the unsteady aerodynamics of the delta-wing orbiter, based upon a detailed analysis of wind tunnel test results, which is reported fully in Part IV (Ref. 9).

Section 2
DELTA-WING AERODYNAMICS

That delta-wing aerodynamics at high angles of attack are dominated by the suction loads generated by leading edge vortices was demonstrated by Örnberg 20 years ago (Ref. 10). The delta-wing aerodynamics have since been investigated extensively, but the investigations have been almost completely restricted to thin wings with sharp leading edges. When one needs information about thick delta wings with rounded leading edges, which is the configuration of interest in regards to the space shuttle, one still has to go back to Örnberg's publication to find a comprehensive treatment of leading edge separation and vortex formation.

Örnberg found in his experiments that the vortex formation on a rounded leading edge starts downstream of the apex (Fig. 1b) rather than at the apex as on a sharp leading edge (Fig. 1a). The starting point moves forward towards the apex with increasing angle of attack (Fig. 2a) in a manner similar to that for the formation of free-body vortices on round-nosed cylinders (Ref. 11). When the sweep angle is decreased to 58 degrees, two (co-rotating) leading edge vortices appear (Fig. 2b). They deviate from regular leading edge vortices in that they bend off downstream before reaching the trailing edge (Figs. 2b and 3a). They are like the so-called part-span vortices observed on swept wings (Ref. 12). (See Fig. 3b.)

It is clear that the unsteady aerodynamics of delta wings with rounded leading edges might be a great deal more complicated than those of sharp-edged delta wings. Even the sharp-edged delta wings are poorly understood when it comes to the unsteady aerodynamics. Thus, it is necessary to first develop the analytic means for description of sharp-edged delta-wing vehicle dynamics. These results can then be used as a reference when describing the effects of leading edge roundness.

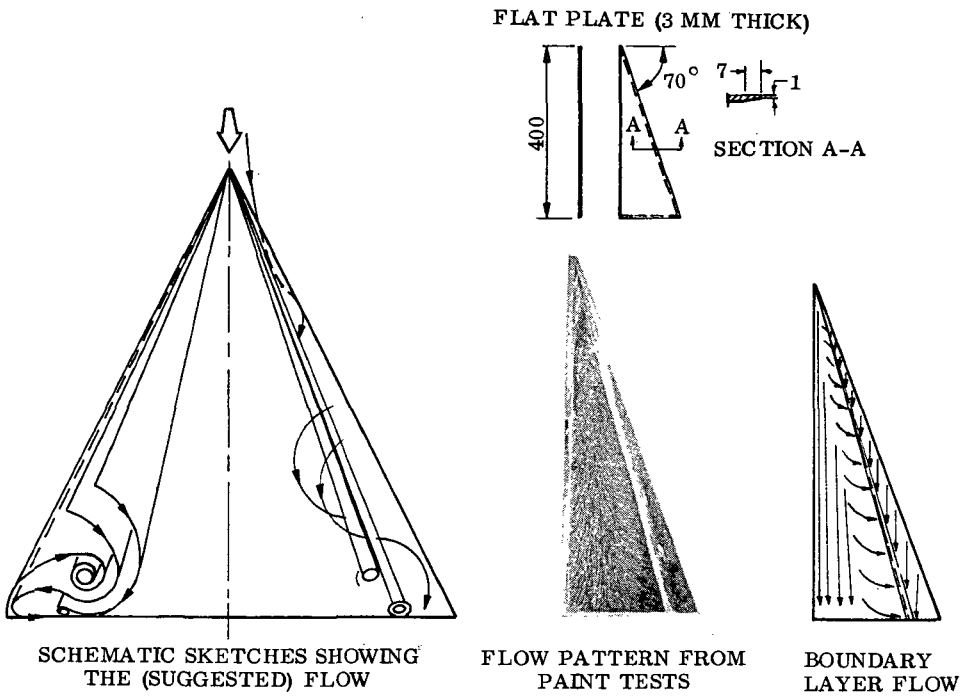

a. FLAT PLATE, SHARP LEADING EDGE

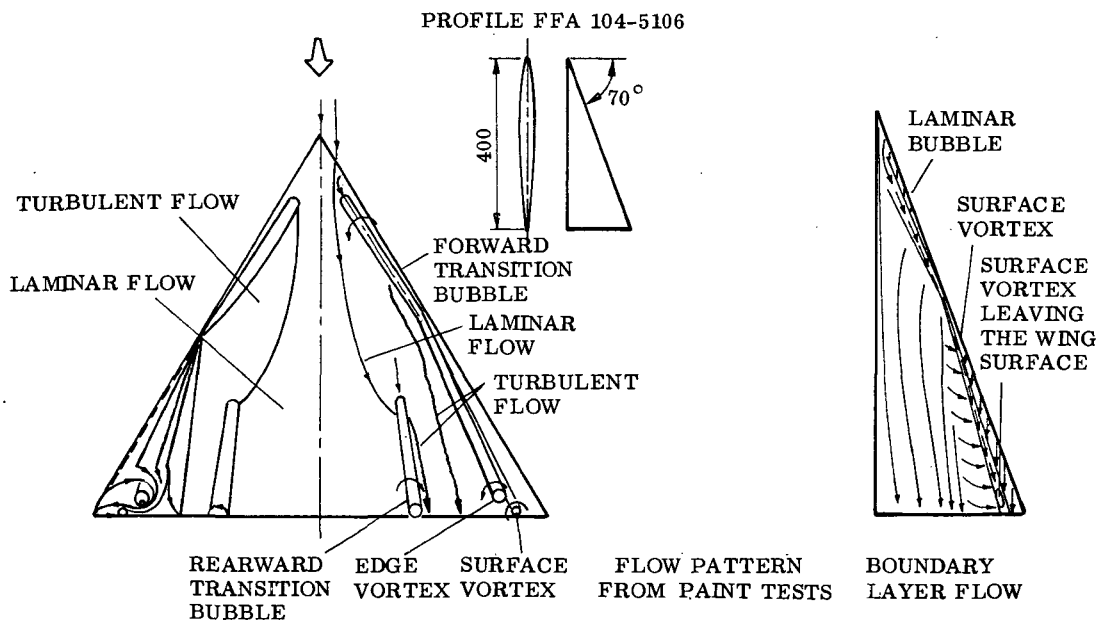

b. 10% THICK, ROUNDED LEADING EDGE

Figure 1. Leeside Flow Patterns on a $\Lambda = 70^\circ$ Delta Wing with Sharp and Rounded Leading Edges at $\alpha = 15^\circ$, $Re = 0.6 \times 10^6$, and $M = 0$ (Ref. 10)

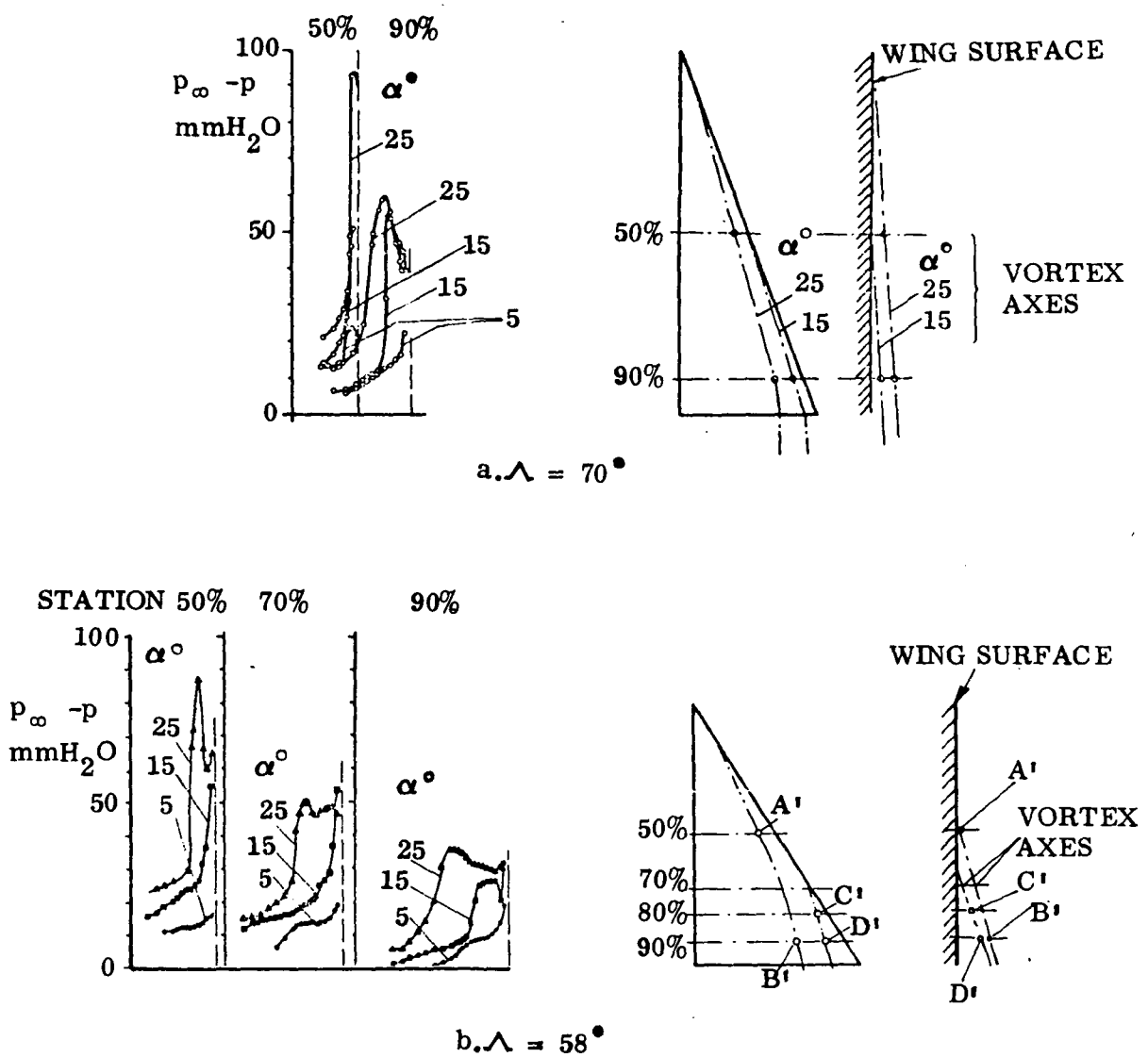

Figure 2. Effect of Sweep Angle on Leading Edge Vortex Formation on 10% Thick Delta Wings with Rounded Leading Edges at M = 0 and Re = 0.6×10^6 (Ref. 10)

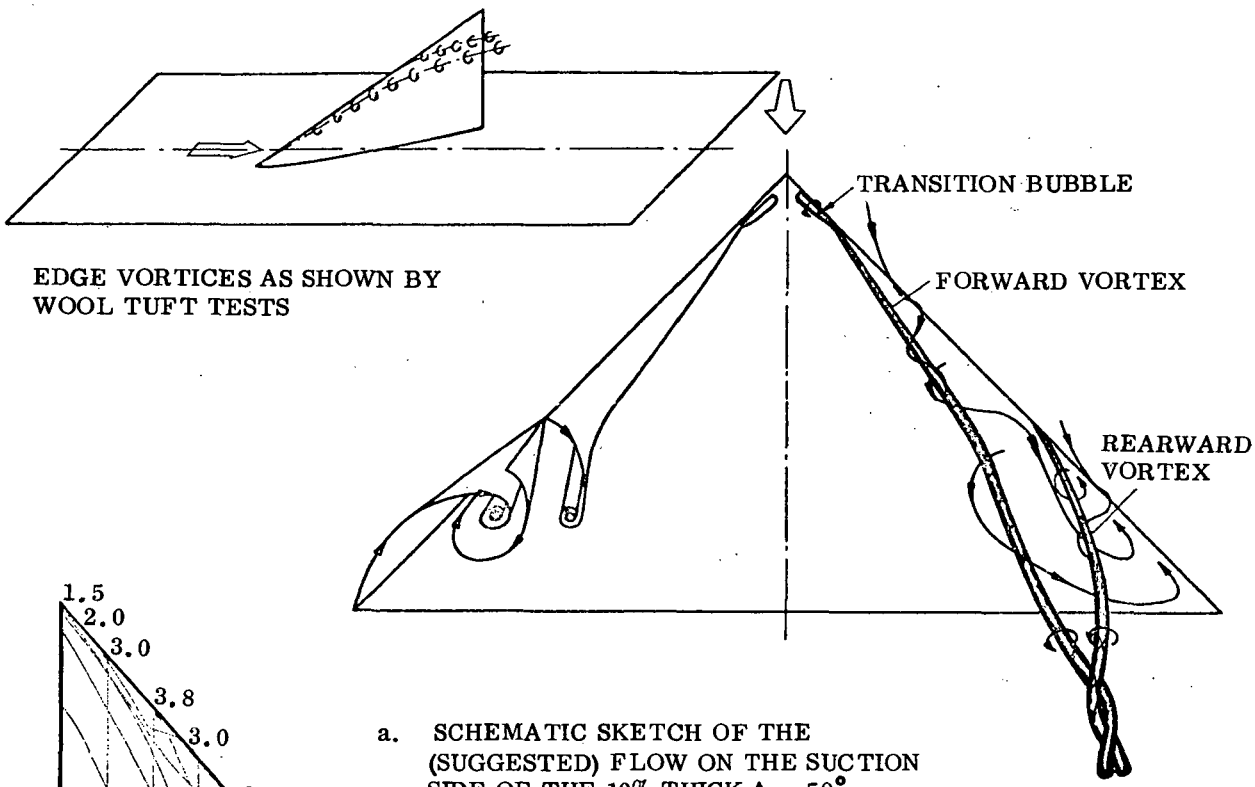

a. SCHEMATIC SKETCH OF THE (SUGGESTED) FLOW ON THE SUCTION SIDE OF THE 10% THICK $\Lambda = 58°$ DELTA WING AT $\alpha = 25°$, M = 0, AND Re = 0.6×10^6 (REF 10)

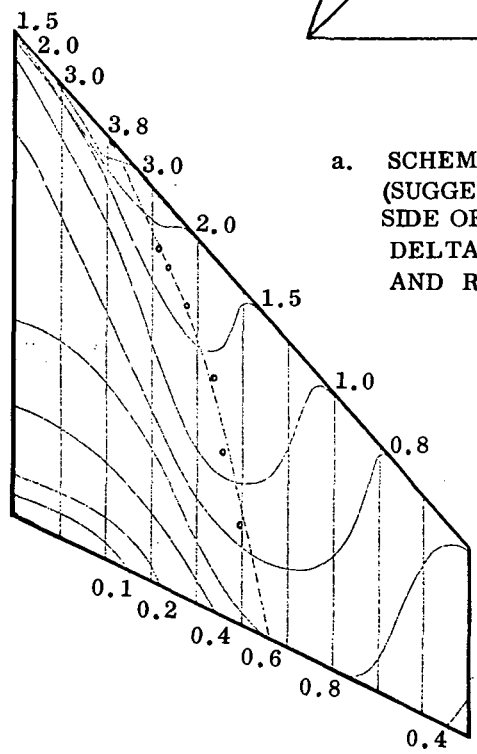

b. UPPER-SURFACE ISOBARS ON A 10% THICK $\Lambda = 49.4°$ CROPPED ARROWHEAD WING AT $\alpha = 20°$, M = 0, and Re = 1.8×10^6 (REF 12)

Figure 3. Partial Span Leading Edge Vortices

Section 3
SHARP-EDGED DELTA-WING AERODYNAMICS

The simple flow concept developed by Polhamus, i.e., the "turned around" leading edge suction, has been remarkably successful in predicting the nonlinear lift generated by the leading edge vortex on sharp-edge slender wings at high angles of attack (Ref. 13). This is true not only for simple delta wings but also for so-called double-deltas as well as arrow- and diamond-shape planforms; and the method also predicts experimentally observed Mach number effects for subsonic leading edge conditions (Ref. 14).

The Polhamus theory has been used as a starting point in the present analysis (Ref. 7) to develop simple analytic means for prediction of the unsteady aerodynamics. The static aerodynamics are predicted well by a modified slender wing theory (Refs. 7 and 15), which, by incorporating some suggestions by Peckham (Ref. 16), leads to a method for universal scaling of the measured delta-wing lift (Refs. 16 through 21) throughout a large angle-of-attack region (Fig. 4). Fig. 5 shows that the present analytic approximation does not worsen the good C_L prediction of experimental data (Ref. 22) already obtained through Polhamus' theory (Fig. 5a) and that it provides a marked improvement of the C_m prediction (Fig. 5b). It is worth noting that the present predictions are good regardless of trailing edge sweep, in sharp contrast to the predictions by the leading-edge-suction analogy with its attached-flow-like longitudinal load distribution. The main difference between the present analysis and available theories is the assumption that the vortex lift distribution deviates substantially from the attached flow load distribution. This has an especially prominent effect on the C_m (C_L) characteristics. Fig. 6 shows that the present analytic approximation gives a decided improvement over the results obtained by strict application of the leading-edge-suction analogy, when trying to predict experimental data trends (Refs. 22 through 24).

The nonlinear unsteady aerodynamics of slender delta wings are analyzed using the method of local linearization by considering small perturbations from a mean static angle of attack (Ref. 7). The total unsteady aerodynamic derivatives are obtained by superposition of attached and separated flow components. The attached flow aerodynamics are computed by application of first-order momentum theory (Ref. 25), modified to agree with the static characteristics given by the developed slender wing approximation for M = 0 (Ref. 7). Fig. 7 indicates that this modified "Slender Body" theory predicts the measured dynamic derivatives at $\alpha = 0$ with satisfactory accuracy over the tested aspect ratio range ($0 < A < 1.5$). At aspect ratios above A = 2, the deviations probably become unacceptable; and a more sophisticated attached flow theory has to be used (see Ref. 26).

The unsteady aerodynamic effects of the leading edge vortices have been obtained using simple analytic theory in combination with static experimental data (Ref. 7). The theoretical results shown in Fig. 8 were obtained only after several modifications to the original analytic formulation, which was based on a direct application of Lambourne's results (Refs. 27 and 28). These modifications are based to a certain extent on empiricism (Ref. 7), and more work is certainly needed before the unsteady aerodynamics of delta wings at high angles of attack can be determined with the desired accuracy. However, the agreement with experimental data (Refs. 29 through 31) is very encouraging and indicates that reliable prediction methods based on a more rigorous theory can be developed.

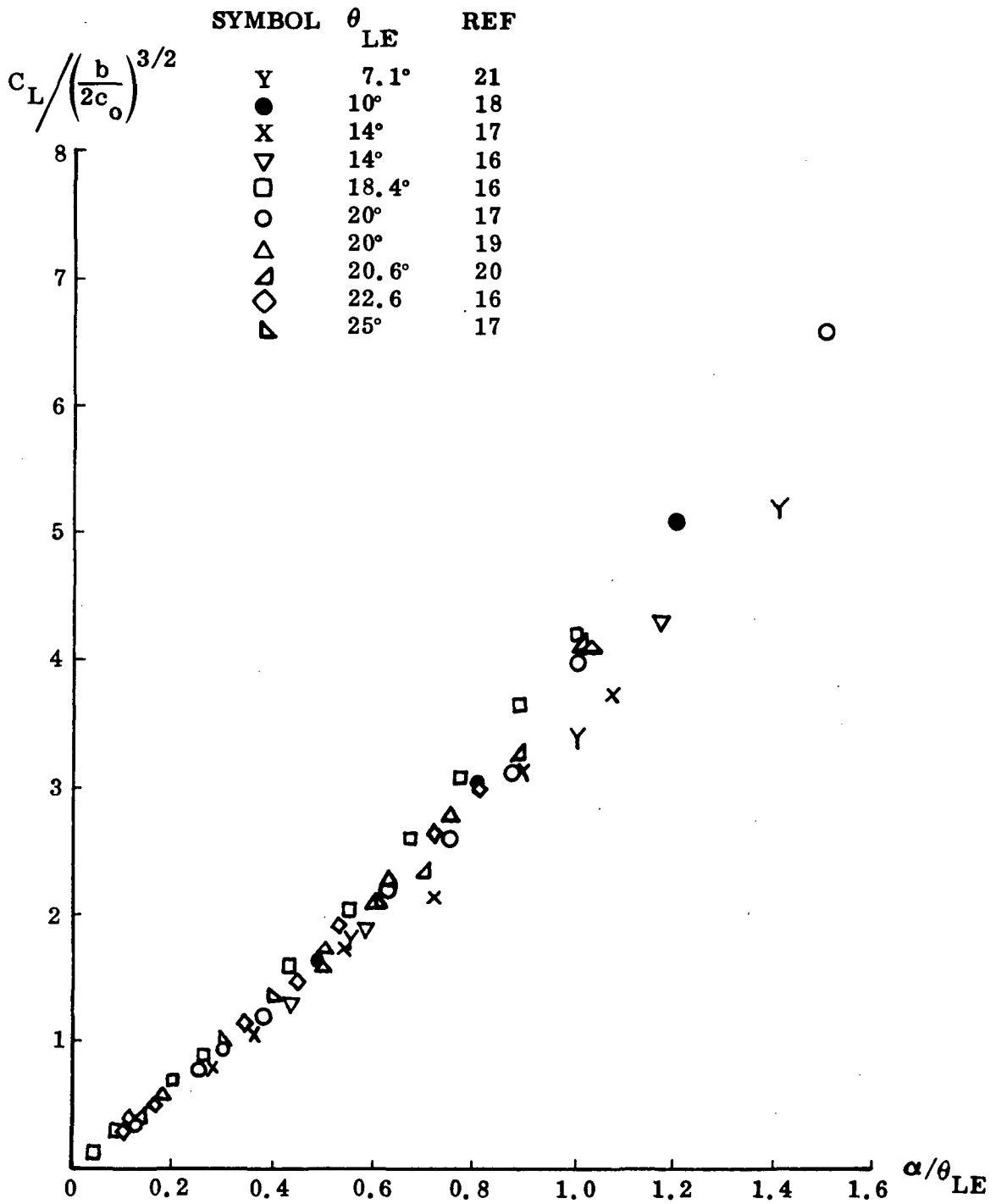

Figure 4. Universal Scaling of Delta-Wing Lift

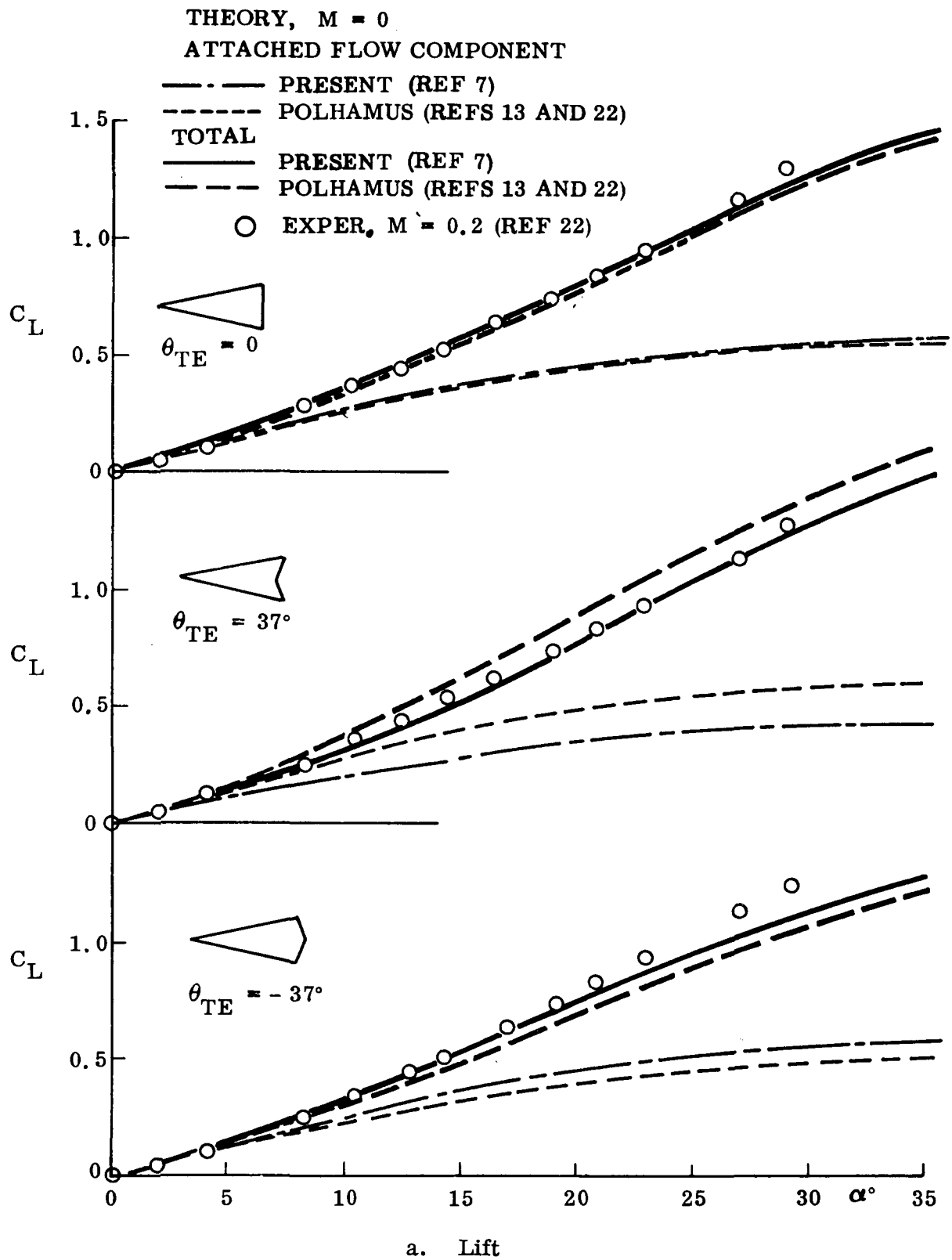

a. Lift

Figure 5. Low Speed Aerodynamic Characteristics of Sharp-Edged Wings with 74° Leading Edge Sweep (Sheet 1 of 2)

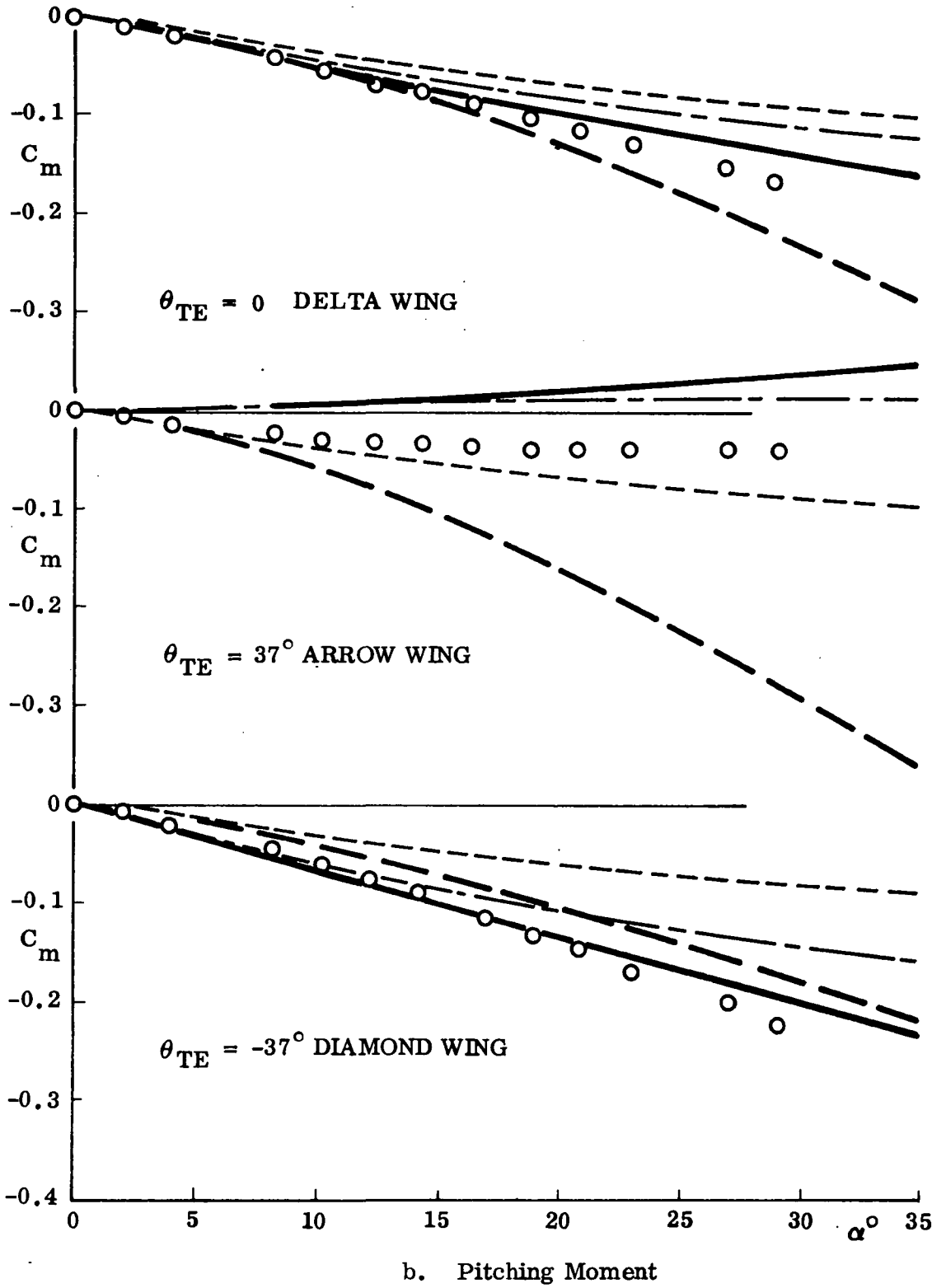

b. Pitching Moment

Figure 5. Low Speed Aerodynamic Characteristics of Sharp-Edged Wings with 74° Leading Edge Sweep (Sheet 2 of 2)

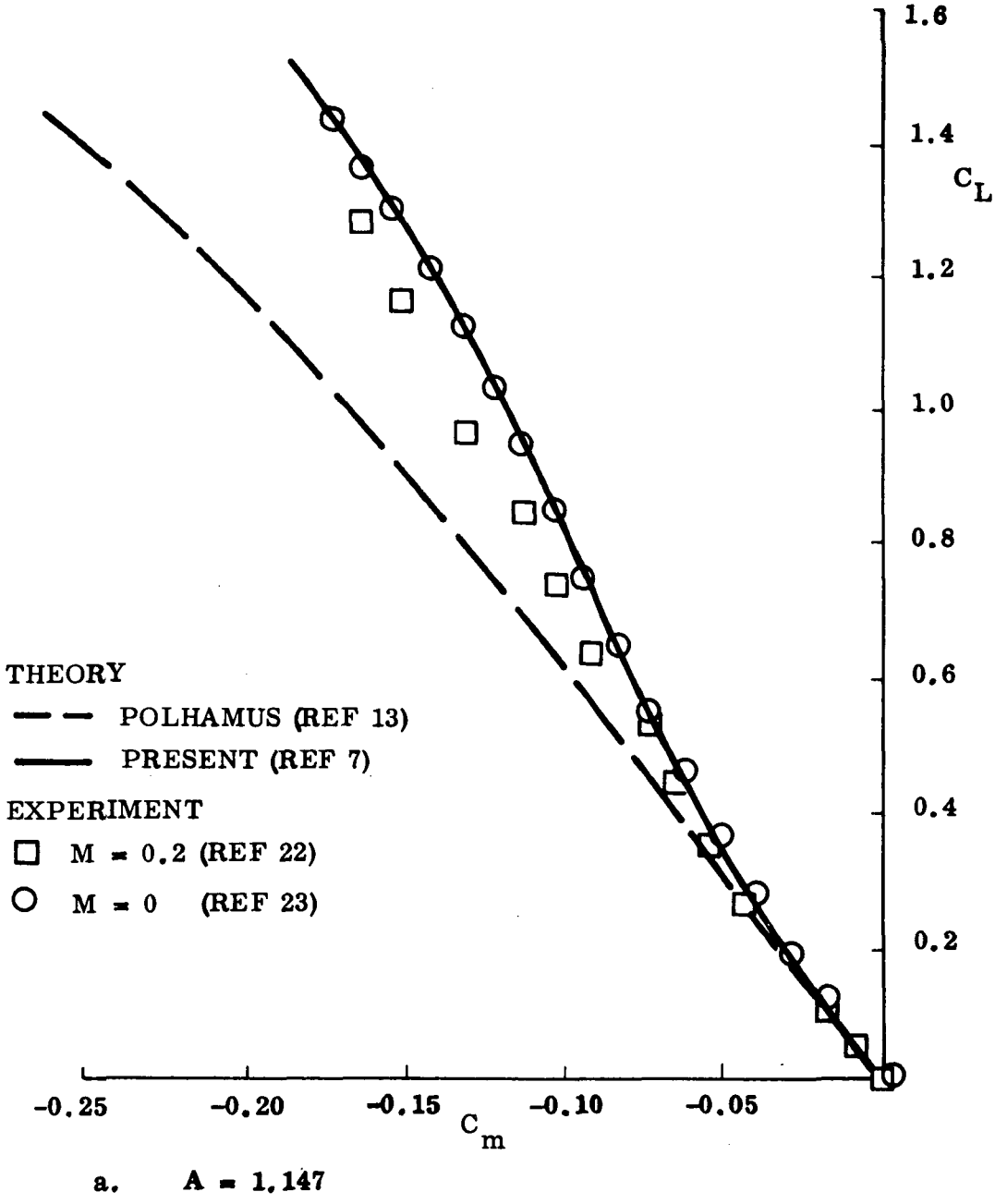

Figure 6. Variation of C_m with C_L for Sharp-Edged Slender Delta Wings (Sheet 1 of 2)

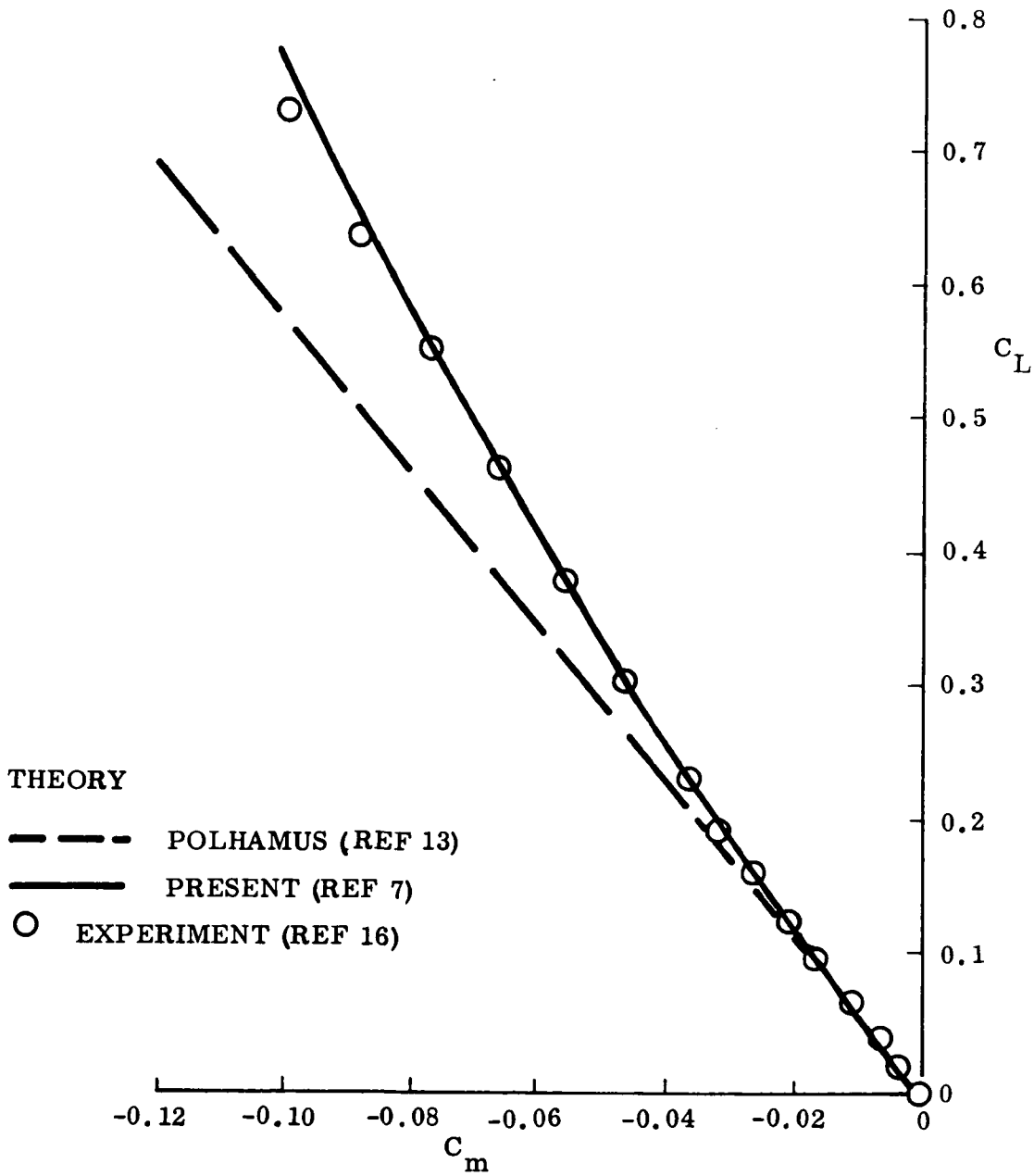

b. A = 1

Figure 6. Variation of C_m with C_L for Sharp-Edged Slender Delta Wings (Sheet 2 of 2)

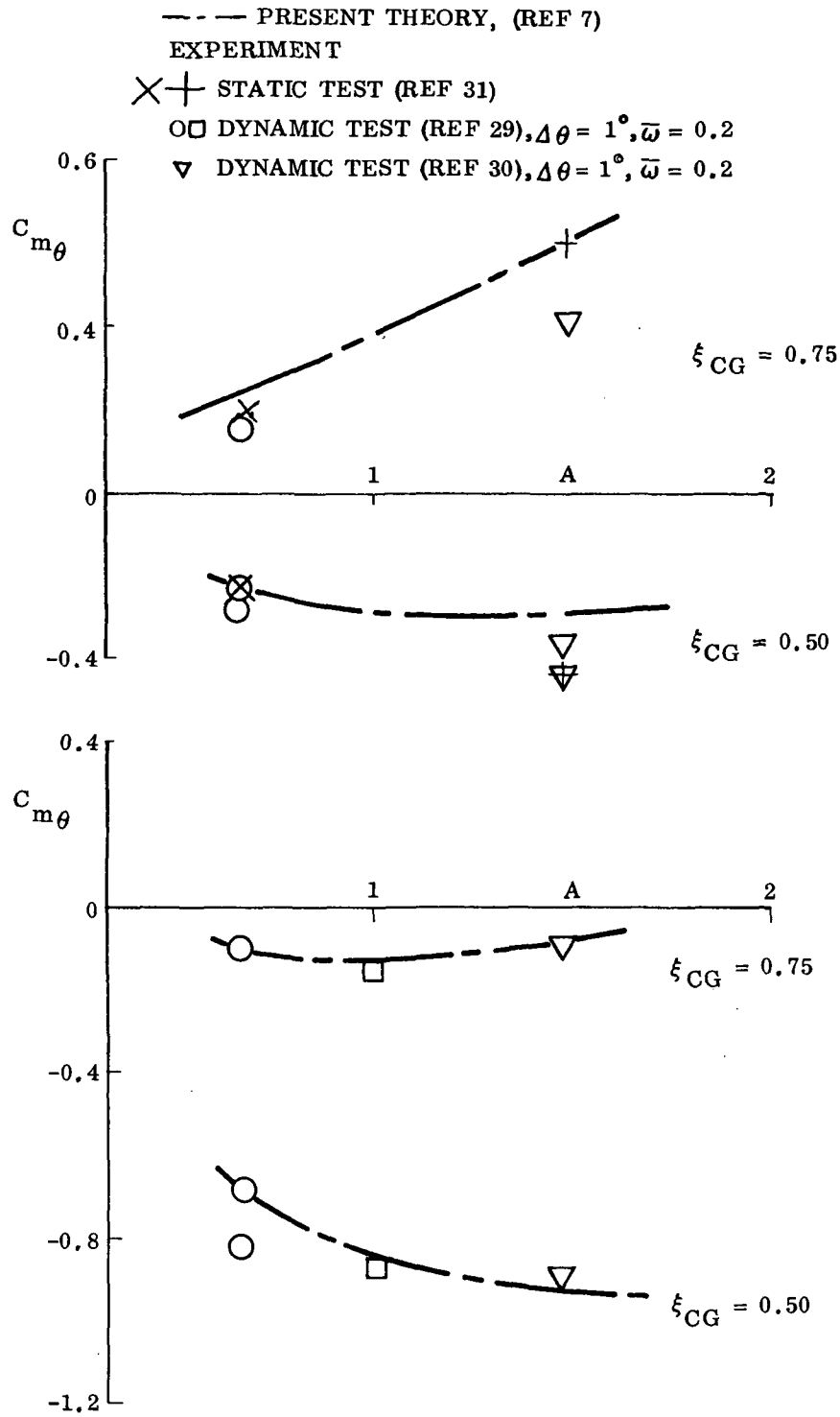

Figure 7. Attached Flow Dynamic Stability Derivatives at $\alpha = 0$ and M = 0

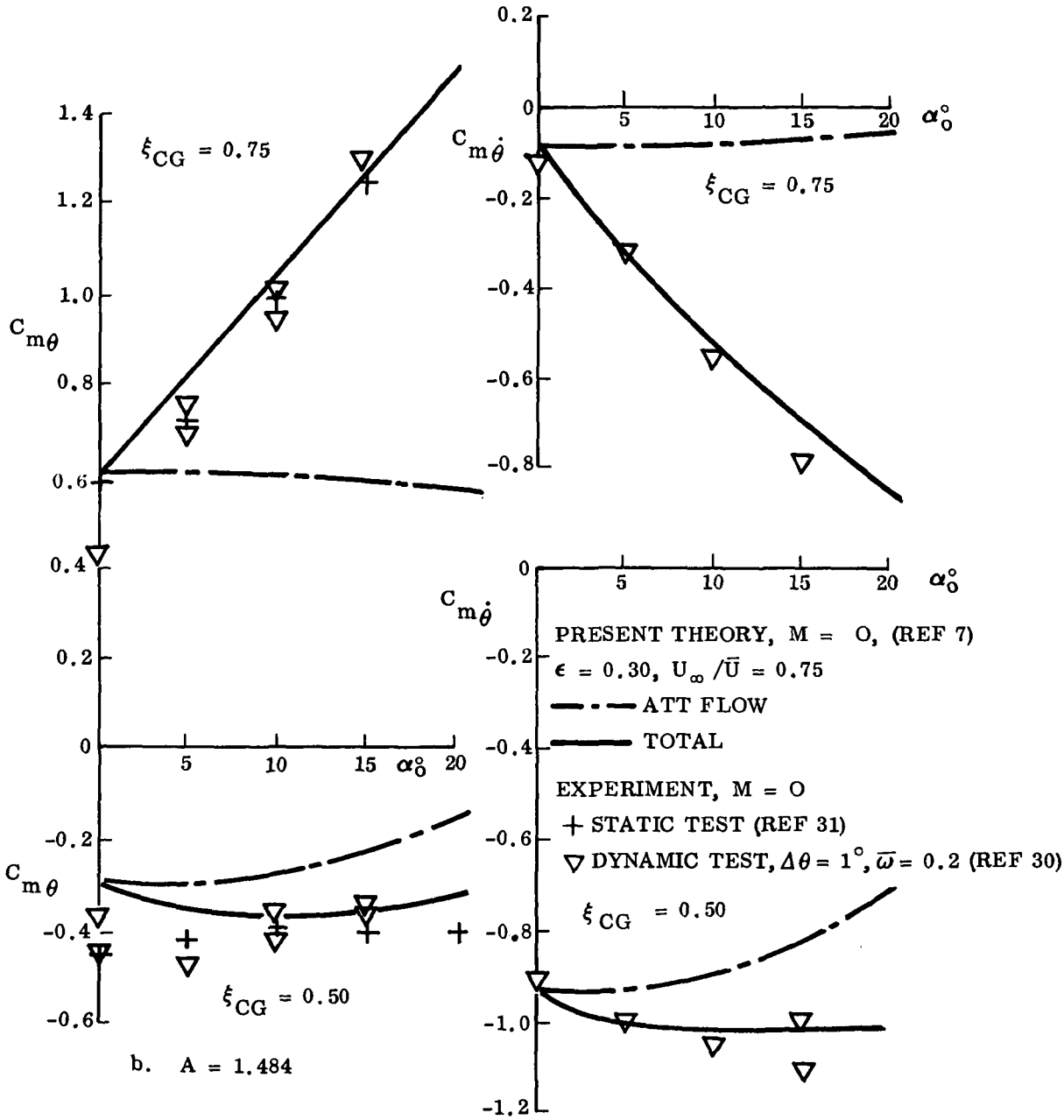

b. A = 1.484

Figure 8. Dynamic Stability Derivatives for Sharp-Edged Delta Wings
(Sheet 1 of 2)

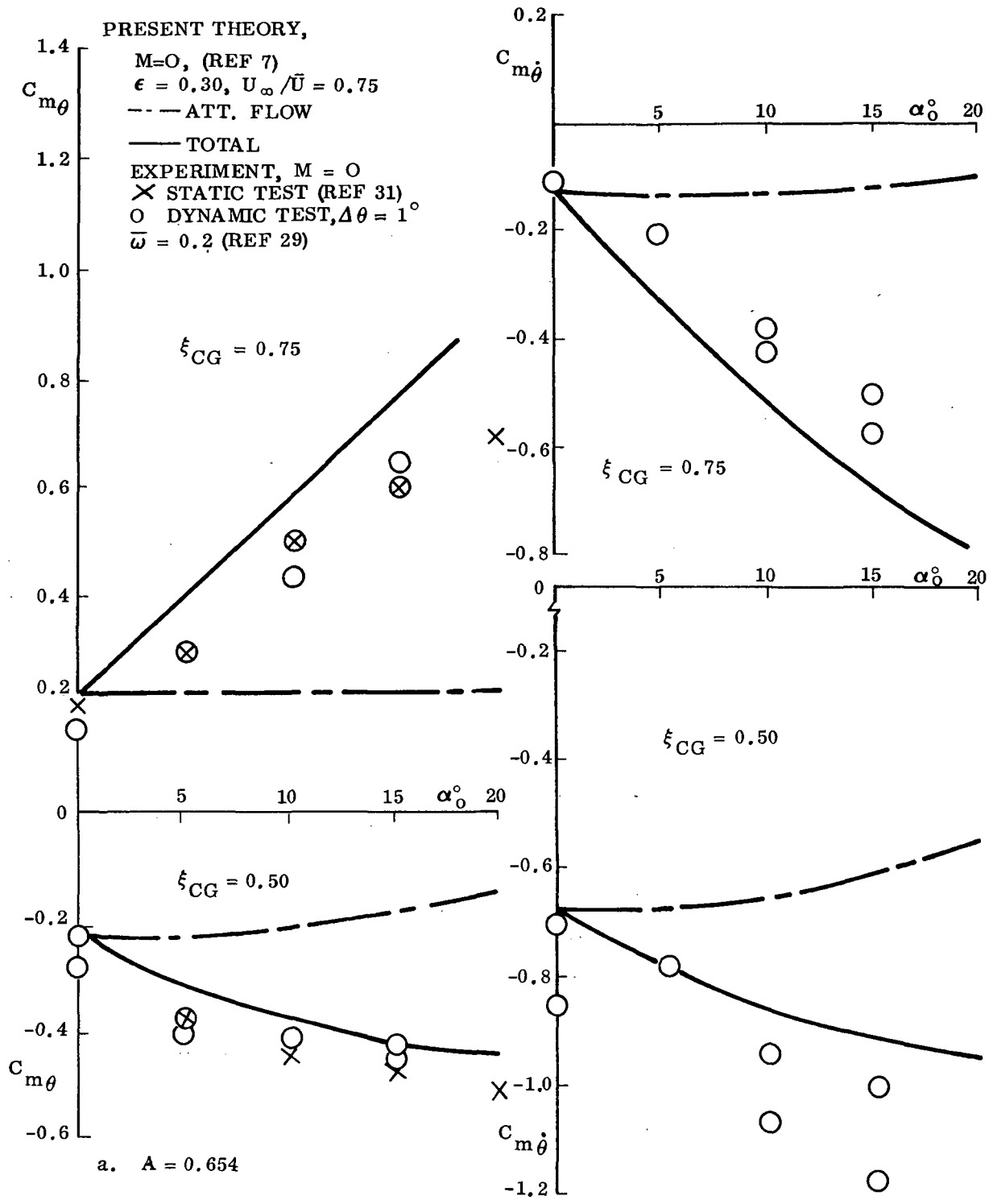

Figure 8. Dynamic Stability Derivatives for Sharp-Edged Delta Wings (Sheet 2 of 2)

Section 4
EFFECT OF ROUNDED LEADING EDGE

Gersten has shown (Ref. 32) that leading edge roundness has a large effect on delta-wing aerodynamics (see Fig. 9). It appears that vortex shedding is delayed until $\alpha \approx 5^\circ$ for the rounded leading edge. Following Ville's suggestion (Ref. 33), one would compute a separation angle $\alpha_{N_S} = 14^\circ$ corresponding to $\alpha_s = 4^\circ$. Applying vortex lift in the usual way (Ref. 7), using an effective angle $(\alpha - \alpha_s)$, gives the results shown in Fig. 10. The simple α_s correction seems to account for most of the effect of leading edge roundness on static characteristics. However, it appears that also the α slope changes, in addition to the α_s shift. This may be tied to the vortex starting point and its movement forward to apex with increasing α, which was shown by Örnberg (Ref. 10 and Figs. 1 through 3).

Woodgate's extensive experiments (Refs. 29 through 31) also covered the effect of leading edge roundness on the delta-wing unsteady aerodynamics (see Ref. 34 and Fig. 11). The same delay of vortex shedding discussed above is also evident in the dynamic results. Again, using Ville's simple analogy (Ref. 33) in combination with the present methods (Ref. 7) gives the results shown in Fig. 12. The static α_s effect also appears to account for most of the effect of leading edge roundness on the dynamic derivatives. This is somewhat surprising, as one would suspect that the additional degree of freedom, i.e., the moving vortex starting point, would amplify the dynamic effects of leading edge separation and be similar to the effect of the moving shock-induced separation on slender "hammerhead" boattails (Ref. 35) and slender cone-cylinder shoulders (Ref. 36).

Thus, it appears that the effects of leading edge roundness on the dynamic characteristics of slender delta wings are much less than expected. Reexamining Örnberg's results (Ref. 10 and Fig. 1b) in view of these measured small effects of leading edge roundness raises the question as to what extent the laminar separation bubble, which stretches all the way from the apex to the vortex starting point, can be

similar to a leading edge vortex in regard to lift generation. If Polhamus' leading edge suction analogy (Ref. 13) is taken into consideration, there should be no real difference. Furthermore, the laminar separation bubble at the leading edge is in most respects similar to the secondary separation on sharp-edged wings (Fig. 1a), which usually is thought to be fully equivalent to a (secondary) vortex.

The "laminar leading edge vortex" is tightened locally at the downstream location where transition takes place. Further downstream the turbulent vortex grows in the usual manner. The transition location is very sensitive to α (Ref. 10 and Fig. 13). This is due, of course, to crossflow effects. The effects of crossflow on transition are well documented for the maximum leading edge radius, i.e., for cones (Ref. 37). One cannot come to any other conclusion than that the leading edge roundness does not seem to fundamentally change the leading edge vortex in regard to its load-generating characteristics. The pinching effect of transition is a second order effect, which possibly can explain the change of α slope discussed earlier in connection with the static characteristics (Fig. 10).

It would be very convenient if the α_s zero shift accounted fully for the effect of leading edge roundness. However, until more data than the limited sample of this study are analyzed, one has to be very cautious in regard to any general conclusions. Much of the experimental evidence on leading edge separation indicates that even minute changes in leading edge curvature can have large effects. For example, airfoil stall data (Refs. 38 and 39), Örnberg's results (Ref. 10), the study of Lambourne et al. on interference problems due to the transducer housing (Ref. 28), and general experience with underside flow fences and vortex generators all indicate that leading edge geometry could have a pronounced effect on the steady and unsteady characteristics of leading edge vortices. More work is clearly needed in this area. Even for sharp-edged delta wings the effects of pure wing thickness are found to be substantial (Refs. 7 and 16). Furthermore, at transonic and supersonic speeds, the leading edge radius has very pronounced effects, as is discussed in the following section.

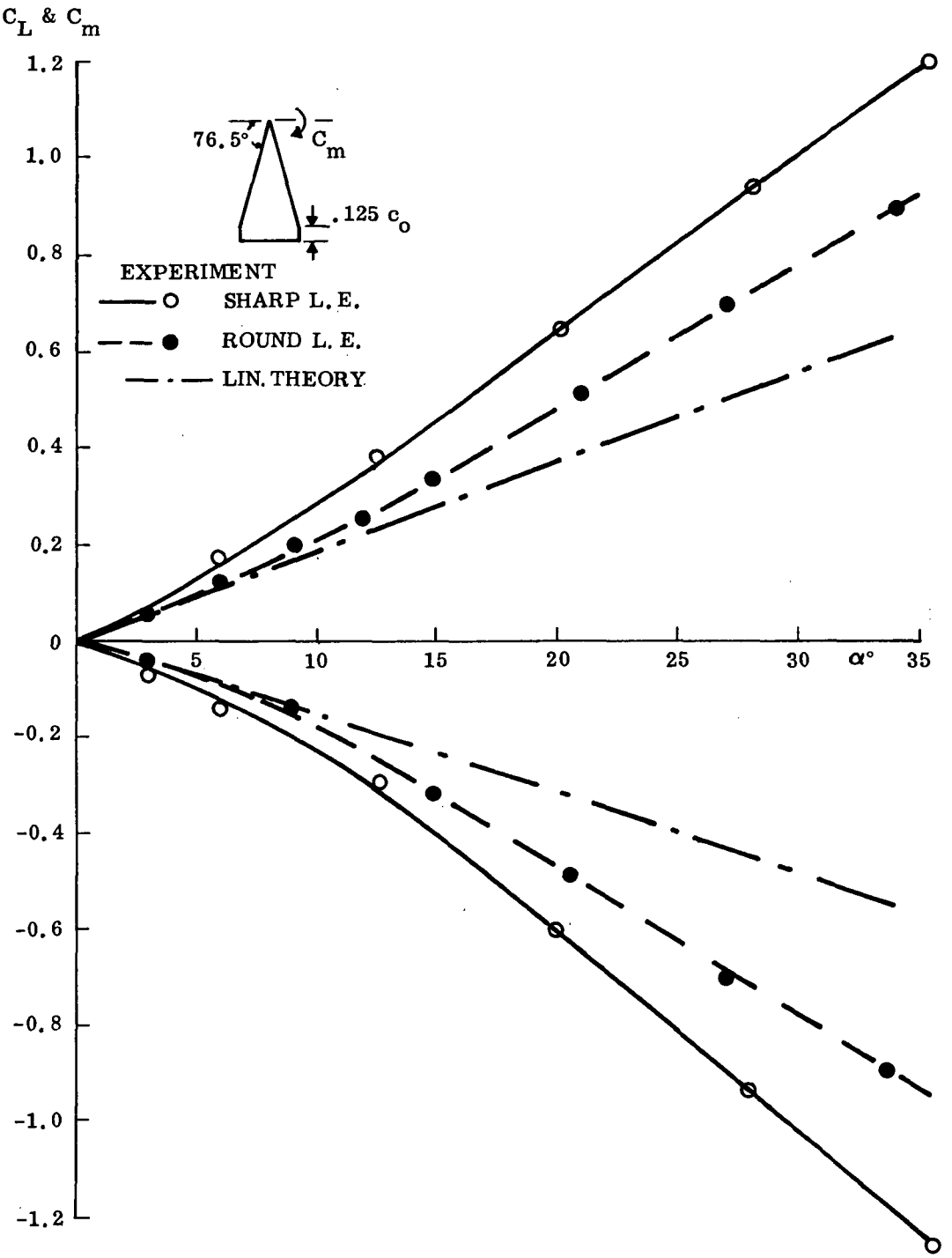

Figure 9. Effect of Leading Edge Roundness on a Cropped $\Lambda = 76.5°$ Delta Wing (Ref. 32)

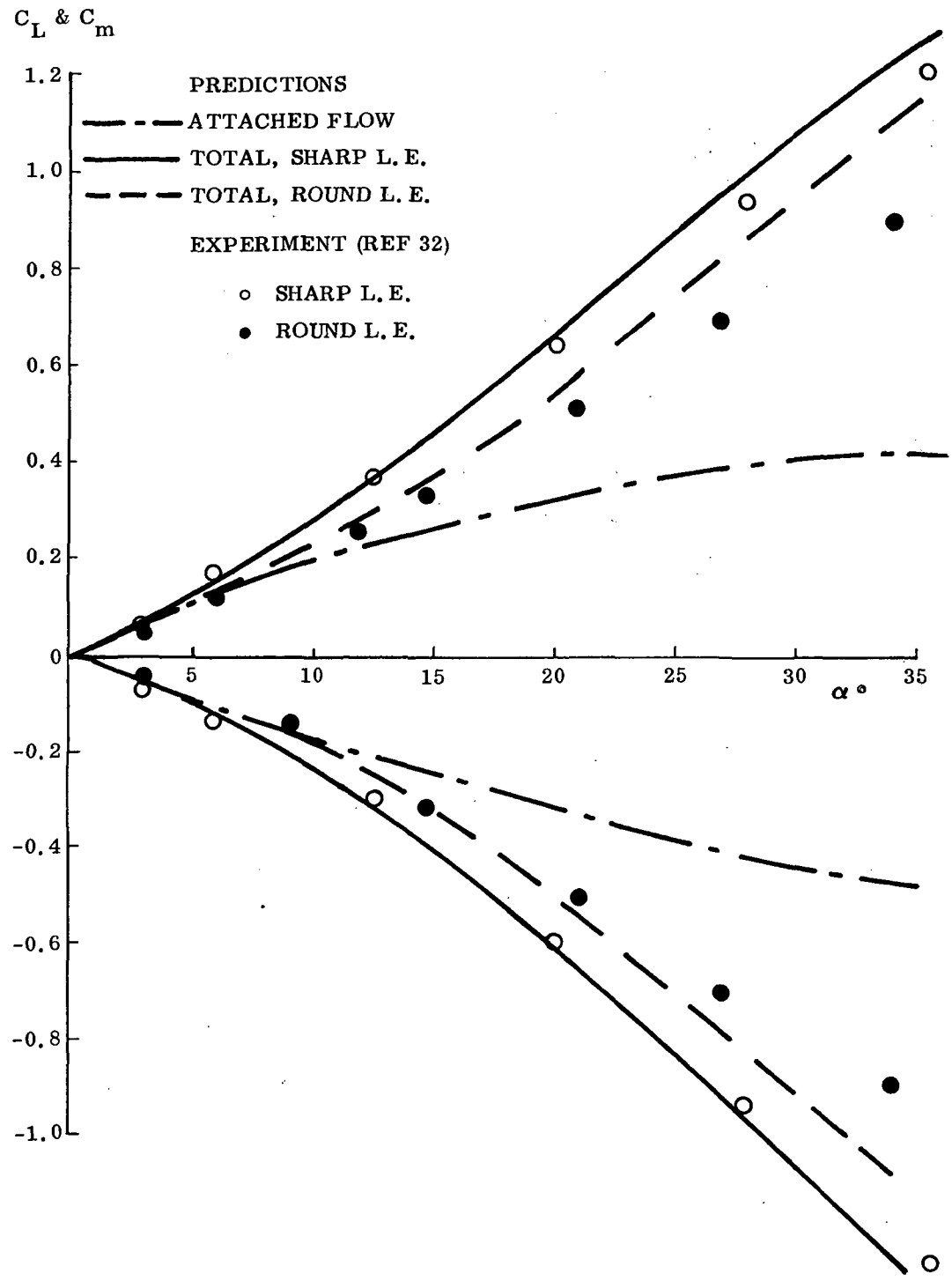

Figure 10. Comparison of Predicted and Measured Effects of Leading Edge Roundness on the Static Characteristics of a $\Lambda = 76.5^\circ$ Cropped Delta Wing

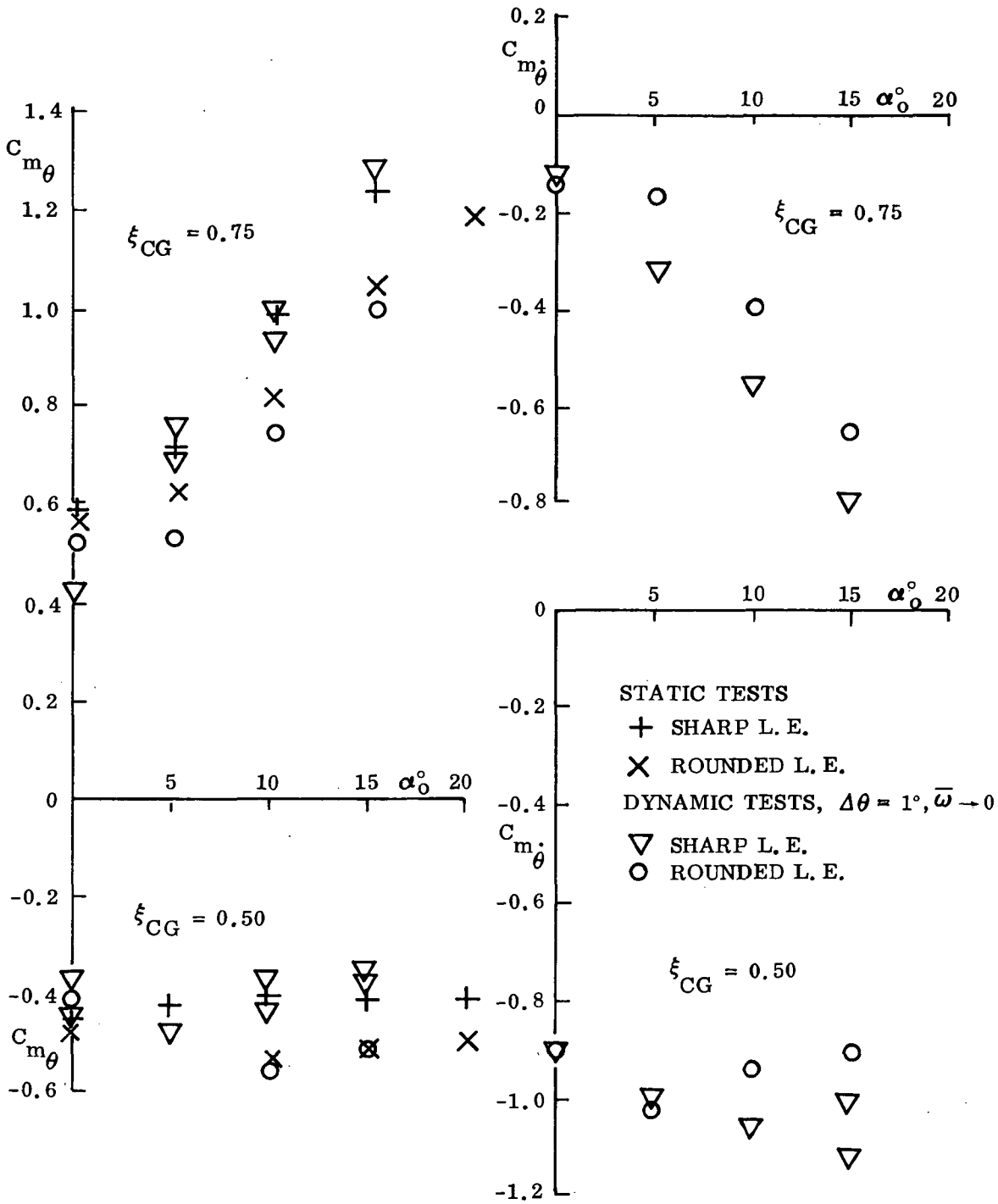

Figure 11. Effect of Leading Edge Roundness on Oscillatory Pitching Moment Derivatives of a $\Lambda = 69.6^\circ$ Delta Wing (Ref. 34)

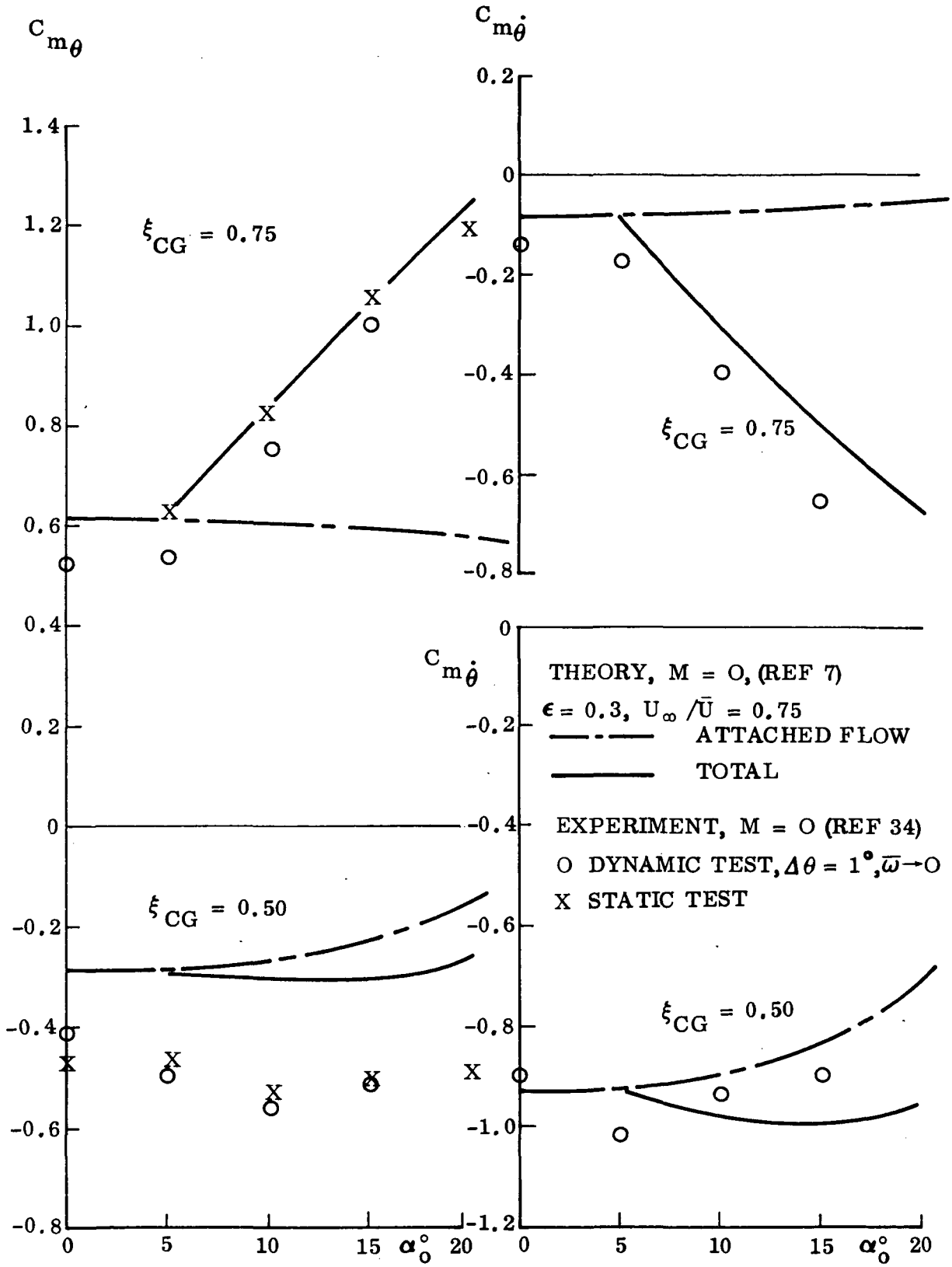

Figure 12. Comparison of Predicted and Measured Dynamic Derivatives of an A = 1.484 Delta Wing with Rounded Leading Edge

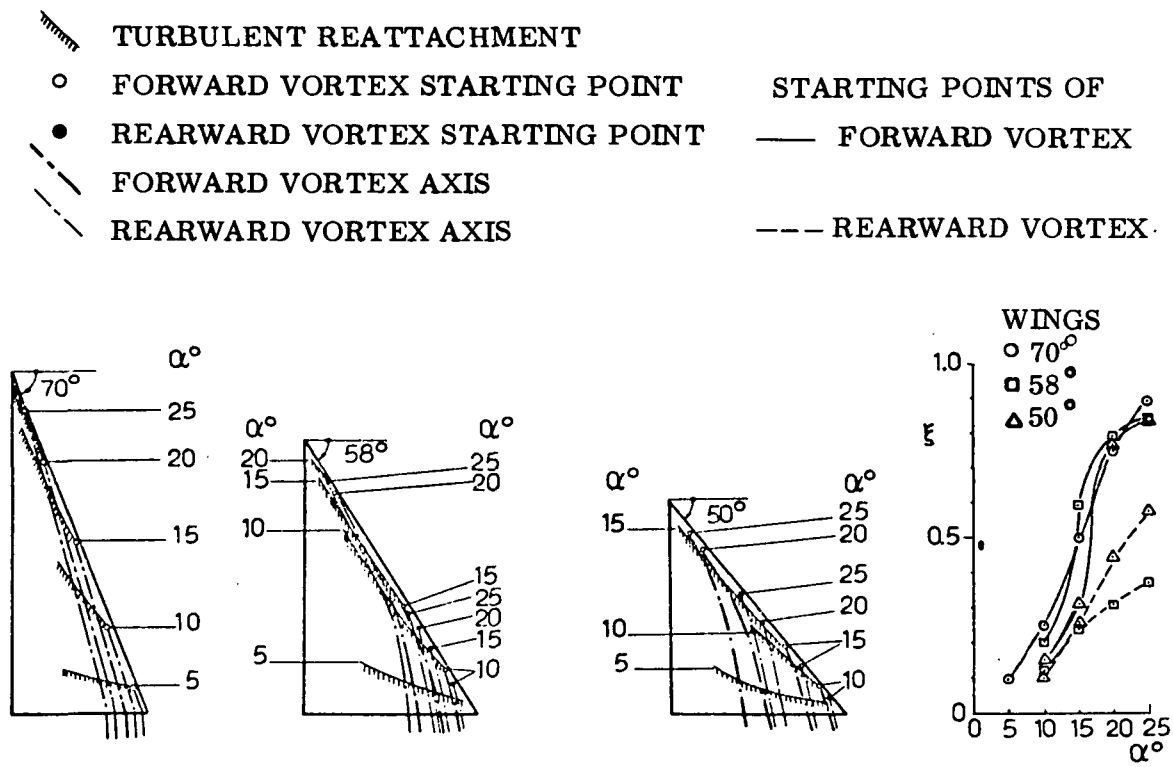

Figure 13. Effect of α on Positions of Transition Regions and Vortices on Three 10% Thick Delta Wings with Rounded Leading Edges at M = 0 and Re = 0.6×10^6 (Ref. 10)

Section 5
MACH NUMBER EFFECTS

When Mach number is increased above $M_\infty = 1$, the leading edge vortex shedding continues as long as the bow shock is detached; but the vortex-induced loads gradually decrease and disappear when the bow shock attaches. This effect of Mach number for the subsonic leading edge is well described by Polhamus' theory (Ref. 14).

When Mach number is large enough to cause an attached bow shock, the delta-wing aerodynamics change character and in many respects become more complicated. Early experimental results on delta wings (Ref. 40) showed that, as the Mach number is increased, the type of flow over the wing (at fixed incidence) changes from that characterized by a leading edge separation, with a coiled vortex sheet lying above the wing, to that in which the flow is attached over the wing leading edge. Squire, Stanbrook, and Jones (Refs. 41 and 42) have investigated how this change takes place at different free-stream Mach numbers, depending upon leading edge sweep angle and leading edge roundness (see Fig. 14). Figure 14 shows that where in the α_N-M_N space this flow attachment occurs depends greatly upon leading edge roundness, and that there exists an α_N-M_N range with mixed separated-attached leading edge flow. One such mixed flow pattern is the part-span vortex shown by Örnberg at low subsonic speeds (Ref. 10 and Fig. 2b). With rounded leading edges there is a tendency for the leading edge separation to occur first near the wing tip and move inboard with increasing angle of attack. This is true throughout the subsonic and transonic speed region. At transonic speeds, a reverse type of mixed separation has been observed by Rogers on a 50° swept wing (Ref. 43 and Fig. 15); and in the low supersonic speed range, Örnberg shows similar attached wing-tip flow on a yawed 63.5° delta wing (Ref. 10 and Fig. 16). This transonic mixed attached-separated flow phenomenon is discussed in detail in Ref. 44 with regard to its potential impact on the orbiter unsteady aerodynamics.

The purpose of the present study is to outline possible analytic approaches for prediction of the unsteady aerodynamic characteristics associated with the various

types of shock-induced separation occurring at transonic, supersonic, and hypersonic speeds. One problem always presenting itself is the computation of the (hypotehtical) attached flow characteristics to which the separation-induced effects should be added (see Refs. 3, 4, 36 through 39, 44 through 48). At subsonic speeds, the modified slender wing theory, Ref. 7, does a good job; and at sonic speeds, the regular slender wing theory (Ref. 15) works well. How far into the supersonic speed range can Jones' theory be used? Using Brown's computations (Ref. 49) produces the results shown in Fig. 17. It appears that for slender wings, $A \leq 1$, Jones' theory would suffice until a theory of similar simplicity can take over, e.g., Newtonian theory (Ref. 50). At hypersonic speeds, leading edge roundness again becomes important and the Newtonian theory cannot be used. However, the embedded Newtonian theory (Ref. 51), which is analytic and almost as simple as the pure Newtonian theory, can supply the attached flow characteristics with the needed accuracy.*

Thus, it appears that the unsteady aerodynamics of the complicated space shuttle ascent configuration can be determined by superposition of the separation-induced effects on idealized attached flow characteristics that can be determined by very simple analytic theories. The separation-induced unsteady aerodynamic characteristics can be determined by using static experimental data in a "lumped-time-history" analytic theory, as has been demonstrated (Refs. 3, 4, 36 through 39, 46 through 48, 52 through 54).

*In work presently being performed at LMSC under contract N62269-73-C-0713, the embedded Newtonian theory will be modified to account for Mach number effects (down to $M = 3$).

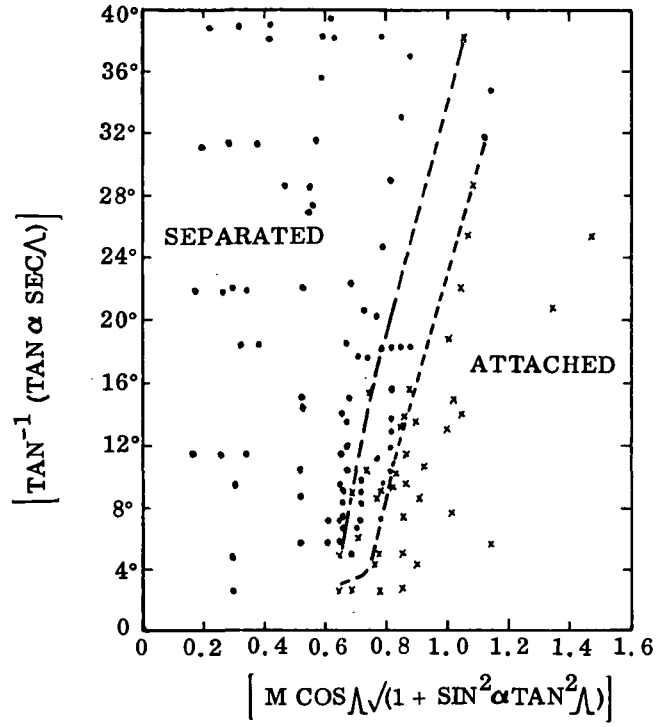

a. SHARP LEADING EDGE

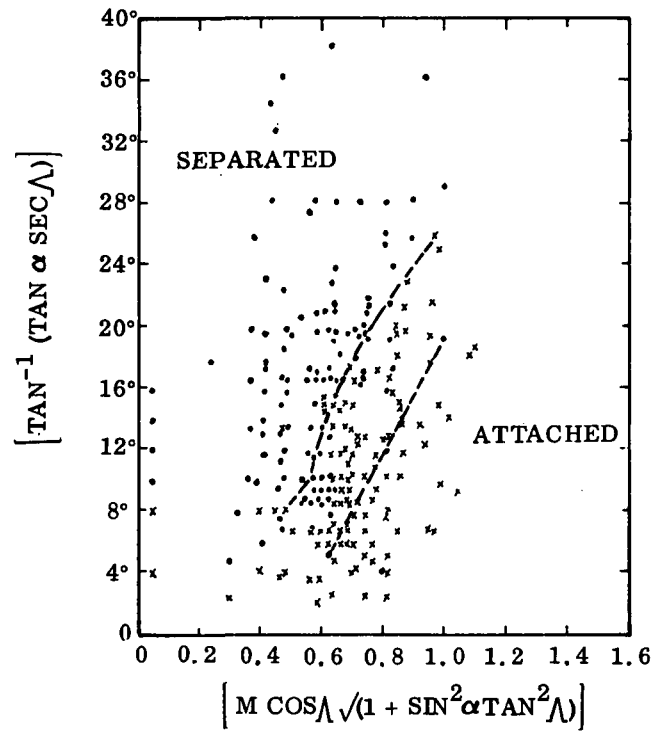

b. ROUNDED LEADING EDGE

Figure 14. α_N-M_N-Boundaries for Leading Edge Flow Attachment (Ref. 42)

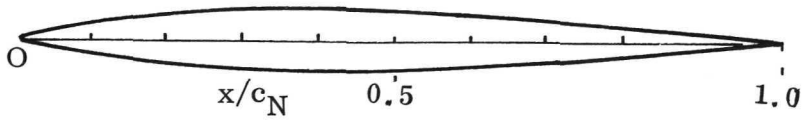

PROFILE OF BASIC SHARP-NOSED SECTION
ALONG CHORD NORMAL TO LEADING EDGE

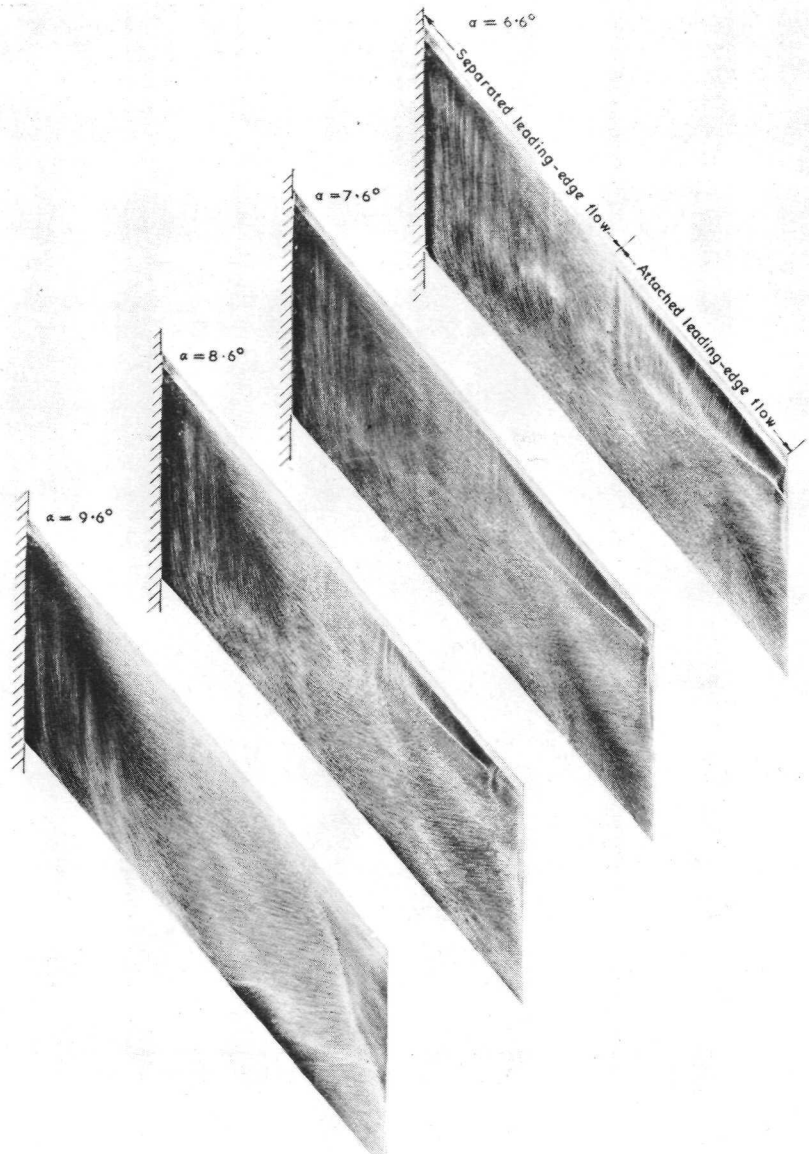

Figure 15. Mixed Leading Edge Flow on an 8% thick 50° Swept Wing with Sharp Leading Edge at M = 1.05 (Ref. 43)

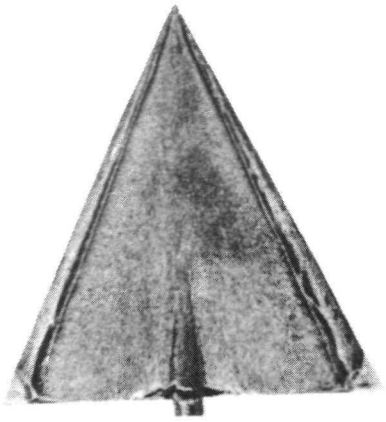

FLOW PATTERN FROM PAINT TESTS

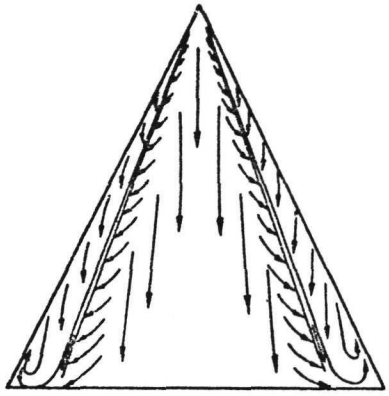

PRINCIPAL FLOW DIRECTIONS IN FLOW PATTERN

a. $\alpha = 8^{\bullet}$ AND $\beta = 0$.

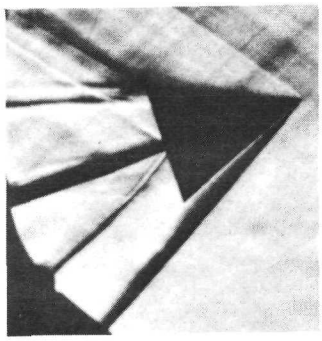

SCHLIEREN PHOTOGRAPH

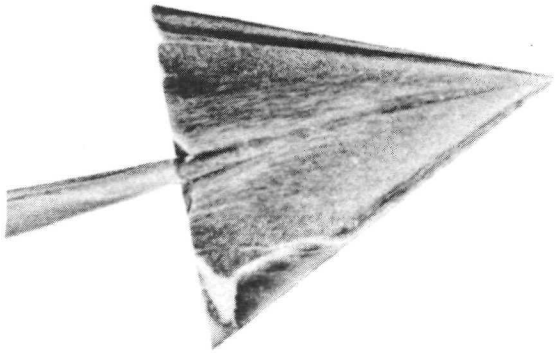

FLOW PATTERN FROM PAINT TESTS

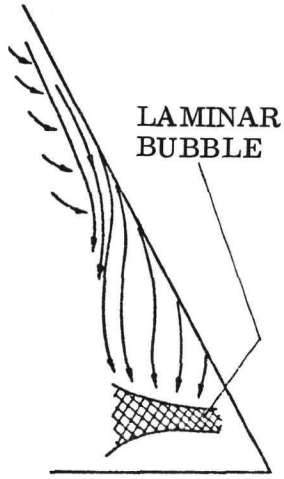

PRINCIPAL FLOW DIRECTIONS IN BOUNDARY LAYER

b. $\alpha = 8^{\circ}$ AND $\beta = 11.5^{\circ}$ WITH MODEL ROLLED 55°.

Figure 16. Attached Leading Edge Flow at the Tip of a $\Lambda = 63.5^{\circ}$ 6.25% Thick Delta Wing with Rounded Leading Edge at M = 1.6 (Ref. 10)

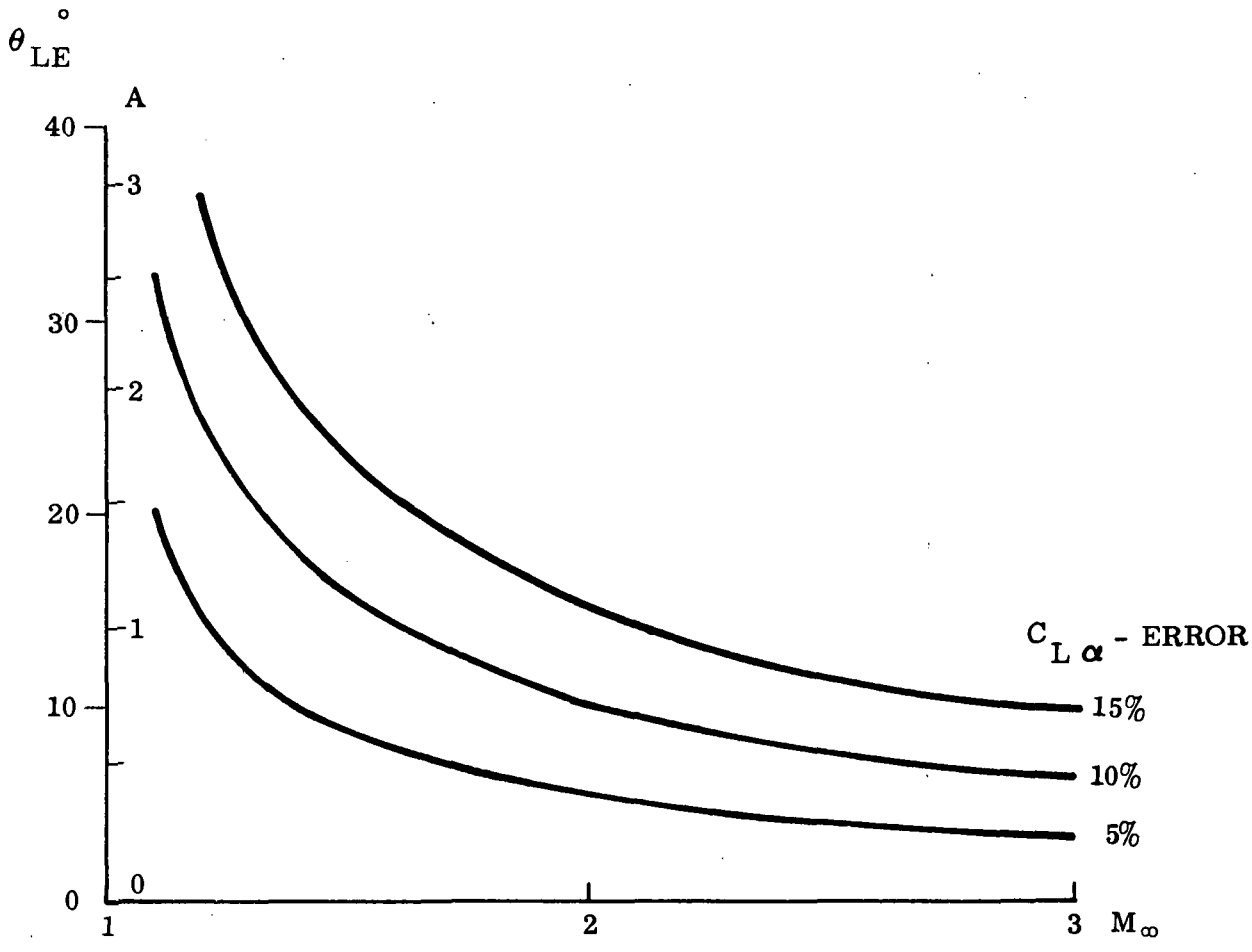

Figure 17. Supersonic Mach Number Range for Application of Jones' Slender Wing Theory

Section 6
BOOSTER INTERFERENCE

The general layout of the shuttle lift-off configuration has not changed drastically within the past year and a half. That is, the booster has consisted of a delta-wing orbiter, external HO tank, and two SRMs in a parallel stage configuration. This similarity is illustrated in Fig. 18, which shows sketches of some representative boost configurations, starting with the original 040A booster and ending with the current configuration. Obviously, these configurations are similar enough that the salient features of the interference flow field will be preserved. Data from three of these configurations (Figs. 18a, 18b, 18c) have been used to gain some insight into the interference flow field and make a preliminary judgement about the impact of the various interference effects on the elastic ascent vehicle dynamics. The interference flow field was examined using oilflow results for the ATP configuration (Ref. 8) and pressure distribution data for the 049 booster (Ref. 55).

The effect of the SRM nose cone on the HO tank flow field is very apparent in the flow sketches derived from the oilflow photographs in Ref. 8 (Fig. 19). At M = 0.9, the channel-like flow between the SRM and the HO tank tends to make the corner pressures more negative, increasing the adverse pressure gradient aft of the shoulder and causing separation at the shoulder of the 17° SRM nose cone, which ordinarily would not experience nose-induced separation (Ref. 56). The separation pockets are vented via pairs of counter rotating vortices, as depicted in the flow sketches. The flow fields for forward and aft SRM positions are similar (compare Figs. 19a and 19b).

At M = 1.46, the SRM bow shock causes a local flow separation for as long as the shock remains nearly normal to the local flow (Fig. 19c). However, as the shock impingement region moves around the HO tank, it becomes more oblique until at some point it no longer separates the flow. At this point, the separation sheds downstream through a pair of vortices on top and bottom of the HO tank. The shock impingement,

however, continues around the body; and another region of separation is formed where the oblique SRM shocks interact with the impinging orbiter bow shock in a manner similar to Edney's type D interaction (Ref. 57). This separation is also vented by a pair of vortices.

When the SRMs are in the forward position, their bow shocks impinge on a portion of the HO tank with high pressures and favorable pressure gradient. A small local separation occurs at the impinging SRM shock, but no separation occurs on top of the HO tank until the orbiter shock is encountered (see Fig. 19d). This separation is now further aft, under the orbiter nose. A region of separation is also generated on the top of the SRM by the lateral extension of the orbiter bow shock. This is relatively independent of SRM position (compare Figs. 19c and 19d).

The flow separations on the retrorocket housing and the leeside orbiter flow field are also depicted in the flow sketches in Fig. 19 to complete the interpretation of the oilflow photographs. These flow fields will not be discussed here; the reader is referred to Ref. 8 for more information.

The SRMs induce a favorable pressure gradient in the region of shock impingement on the HO tank (Refs. 8, 55), an effect that increases with α as the SRM expansion grows with α. Thus, the shock-induced separation tends to vanish with α, opposite to the usual trends of shock-induced separation (Refs. 58 and 59). Similar effects occur on the SRM. The result is that owing to the shock-induced separation, the HO tank load is dependent upon flow conditions at the SRM shoulder. It is less clear, however, how much of the SRM load is induced. Obviously, the attitude at the SRM shoulder sets the initial separation and vortex asymmetry, but the local crossflow may also play a part in determining the vortex asymmetry. Thus, when the effective elastic damping derivative was calculated using the analytic methods of Refs. 3 and 4, the shoulder loads were allowed to vary all the way from entirely induced to entirely local (Fig. 20). The potential of negative damping seems possible enough to warrant further investigation, especially since it appears that negative damping could occur over a significant range of the supersonic Mach numbers investigated.

A preliminary study of the effect of the exhaust plumes of the SRM and orbiter engines showed that the plumes, simulated by solid bodies, could cause a significant alteration of the booster stability (Ref. 60). Dods et al. have obtained qualitatively similar results for gaseous plumes (Ref. 61).

It has been postulated in Ref. 8 that the bulk of the plume-induced effects at $\alpha = 0^\circ$ are the result of plume-induced separation between the booster and the orbiter. The postulated flow model resulted from an analysis of the plume-induced booster loads (Ref. 61). Further corroborating evidence is furnished by unpublished oilflow photographs from the investigations by Dods et al. that show a large region of separation on the bottom surface of the orbiter wing for $-4^\circ \leq \alpha \leq 2^\circ$ and little or no effect on the upper surface. Henderson has published one of the Dods oilflow photographs in Ref. 62, showing a nearly negligible plume-induced leeside flow separation at the very trailing edge of the orbiter wing at $\alpha = 4^\circ$, $M = 1.6$. A sketch of the postulated plume-induced flow field is shown in Fig. 21. When the booster is pitched, the vortices that are shed by the various separated flow regions (Fig. 19) expand to the leeward. The flow entrained by these vortices, assisted by the local flow jetting through the SRM-HO tank gaps, tends to suppress the plume-induced separation, as it did for the separation generated by the SRM flare (Ref. 8). The separation shrinks with α, as illustrated in Fig. 21. The result is a decreasing wing load. Yawing the booster skews the separation to the leeward. The separation becomes asymmetric on the booster, expanding on the leeward SRM. The booster vortices cause a reduction in the flow separation on the wing adjacent to the HO tank, just as they did for the SRM-induced flow separation (Ref. 8). However, the exhaust plume, which is large and directed outboard, involves a significant separation at the wing tips. This tip separation expands, along with the general expansion of the separation, on the leeside of the booster. The separation probably also contracts on the windward wing due to local crossflow effects. These tip effects dominate the rolling moment (Ref. 8).

The preceding flow model is highly speculative. It does, however, fit the available flow visualization evidence; and it explains the plume-induced forces (Refs. 8, 60, and 61). It also allows one to make some judgement on the important factors affecting the unsteady aerodynamics of the plume-induced loads: the pertinent crossflow

influence point and the convection speed. For example, the induced normal load $\Delta^i C_{N_{\alpha_P}}$ is largely the result of the crossflow at the SRM shoulder since it sets the expansion-separation asymmetry, with associated vortex strength and position. However, $\Delta^i C_{N_{\alpha_P}}$ is also somewhat a function of the flow below the wing jetting through the SRM-HO tank gap. This can be assumed to happen instantaneously compared with the convection of vortex effects. (The vortices can be assumed to be convected downstream with freestream velocity (Ref. 7)). Obviously, it is only possible to make an order-of-magnitude estimate of the effect of the plumes on the aeroelastic stability of the shuttle; and to make such estimates involves even a little more "reaching." Since the only structural deformation modes available to the authors are for the 049 booster (Ref. 63), it must be assumed that the plume-induced loads for the 040A and the 049 are the same. Fig. 22 presents the aerodynamic damping of the 049 booster in percent of critical for the 3.64-Hz symmetric mode (calculated using the methods of Refs. 3 and 4). These values include the combined effects of solid exhaust plumes and flow separation on the booster (Fig. 20). The necessary trajectory information was obtained from Ref. 64. It should be emphasized that any unsteady aerodynamic effects on the orbiter due to interference effects other than the exhaust plumes have not been included. If one assumes the usual rule of thumb, i.e., a value of 1 percent of critical for the structural damping (±0.5%), it is apparent that the aerodynamic undamping comes dangerously close to dominating the structural damping. Thus, the shuttle booster could experience undamping of this particular elastic mode.

The preceding results were for solid fairings simulating the exhaust plumes. Naturally, the question of how well the solid plumes simulate real life gaseous plumes is pertinent. Dods et al. (Ref. 61) show that, at M = 1.6, their solid plumes come very close to simulating the gaseous plumes. However, there is a significant difference between the solid-plume effects of Dods et al. and Brownson et al. (Ref. 60). The most significant difference between the two tests was that Brownson measured the loads on the booster, including those on the SRM nozzles; whereas Dods could not include the loads on the nozzles, since they were part of the gas supply plumbing. Other model differences involved are considered relatively minor compared to the nozzle loads (Ref. 8).

These effects are illustrated on Fig. 25 which shows a comparison of damping results at M = 1.6 (the only common Mach number) for the three cases: solid plumes with nozzle loads, solid plumes without nozzle loads, and gaseous plumes without nozzle loads. If the nozzle loads are assumed to be the same, it appears that for gaseous plumes the aerodynamic undamping is still dangerously close to overtaking the structural damping. Of course, these results are only approximate. However, they do show that undamping is possible; and they indicate, therefore, that the problem requires further investigation. As stated previously, these estimates do not include any unsteady flow effects on the orbiter other than the plume effects. Ref. 8 shows that the vortices from the nose-induced flow separation over the retrorocket housing on the HO tank can affect the orbiter, as can the other booster vortices at angle of attack. Furthermore, the current configuration with the SRMs in the normal position has a greatly expanded region of flow separation forward of the orbiter. All these effects could contribute further towards negative aerodynamic damping.

Dods et al. obtained a vapor screen photograph during the gaseous plume tests (Ref. 61) that has some interesting implications (Fig. 24). The photograph shows SRM and orbiter plumes 15 inches aft of the model at M = 1.6, $\alpha = -4^\circ$ (orbiter $\alpha = -7^\circ$). Traces from the orbiter-wing leading edge vortices are evident in the upper outside edge of the SRM plumes. It is not too difficult to imagine the exhaust plumes having an effect similar to Hummel's obstruction (Ref. 65), thus causing burst of the orbiter leading edge vortices which could result in discontinuous changes in the aerodynamic characteristics. At $\beta \neq 0$, the effects would be felt by the moments about all three stability axes, as burst occurs first on one wing. Burst in itself is not always serious, as was discussed in connection with the delta-wing dynamics (Refs. 7, 44, 66, and 67). However, the possible encounter of discontinuous (on-off) stepwise loadings due to vortex burst could seriously degrade the aerodynamic damping. Again, this only serves to point out the need for further investigation before a safe ascent of the shuttle can be assured.

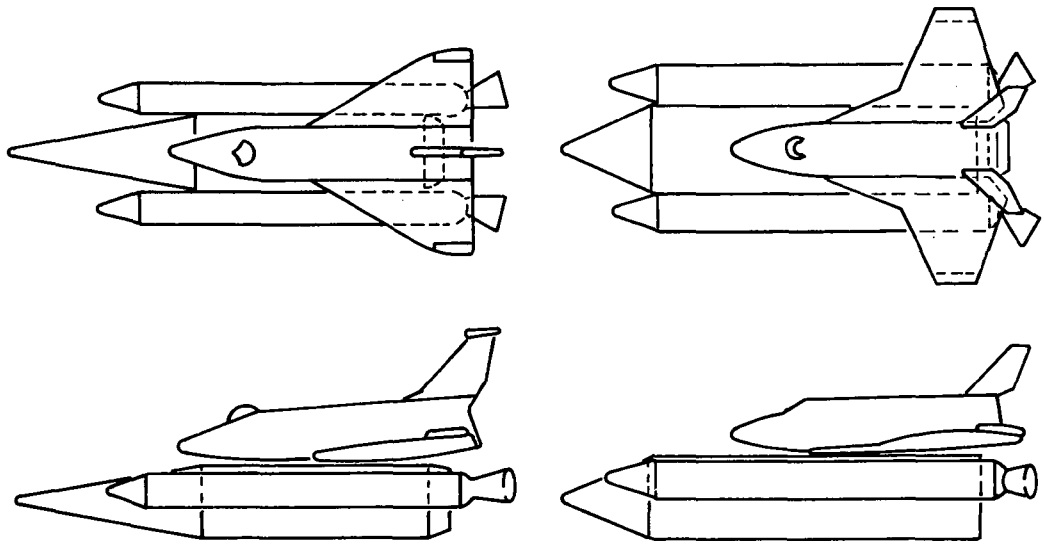

a) 040 A CONFIGURATION

b) 049 CONFIGURATION

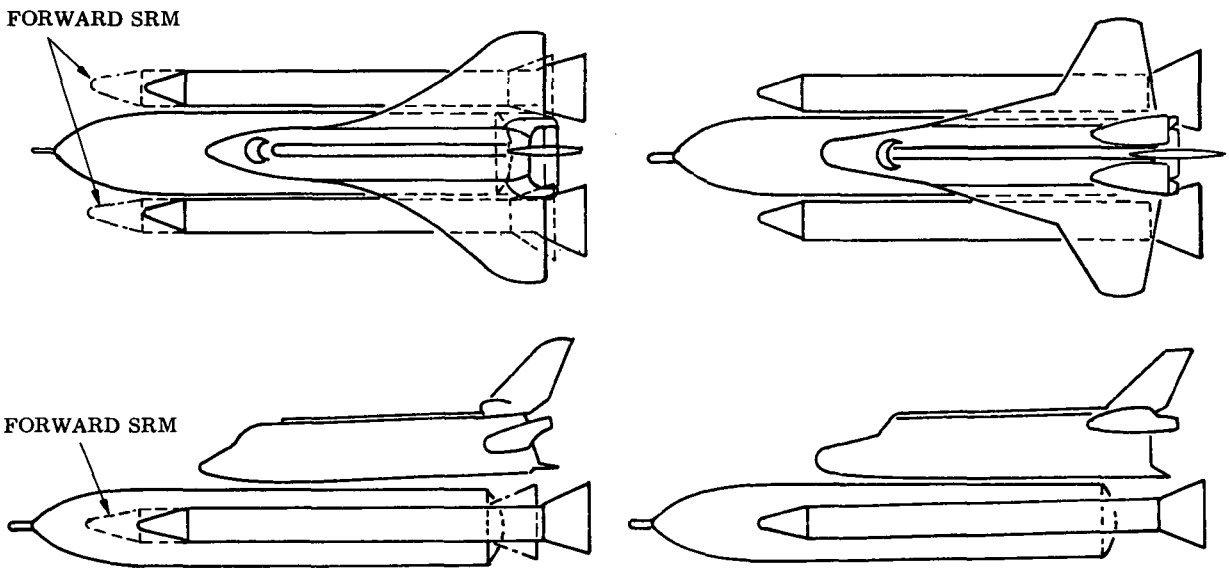

c) ATP CONFIGURATION

d) CURRENT CONFIGURATION

Figure 18. Space Shuttle Lift-Off Configurations

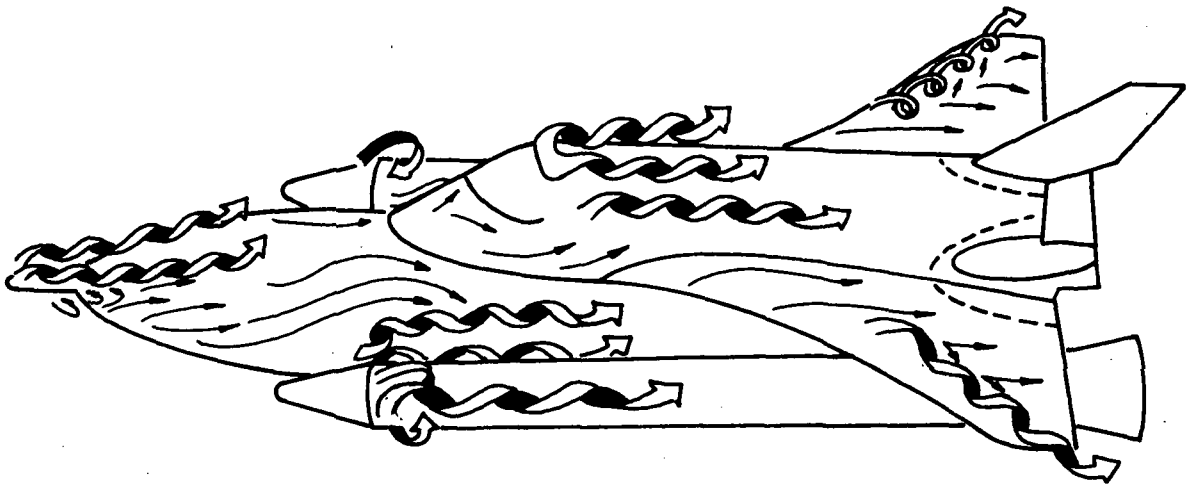

a. NORMAL SRM, M = 0.9

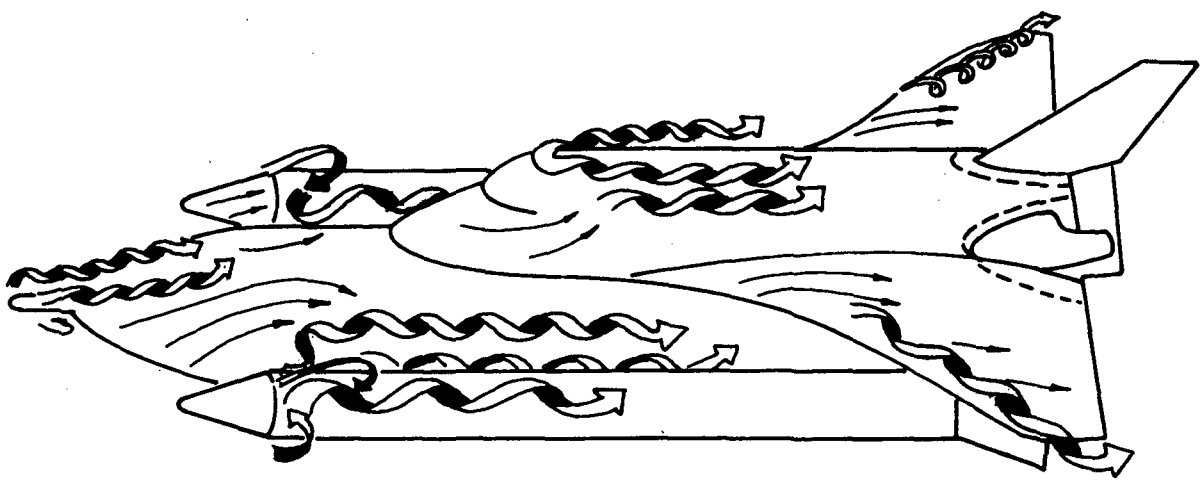

b. FORWARD SRM, M = 0.9

Figure 19. Interference Flow Field (Sheet 1 of 2)

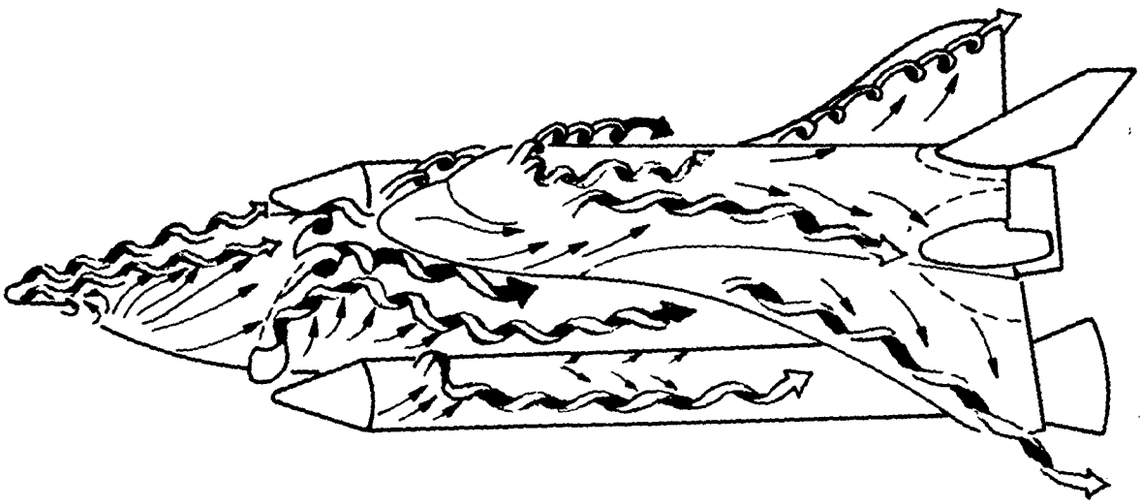

c. NORMAL SRM, M = 1.46

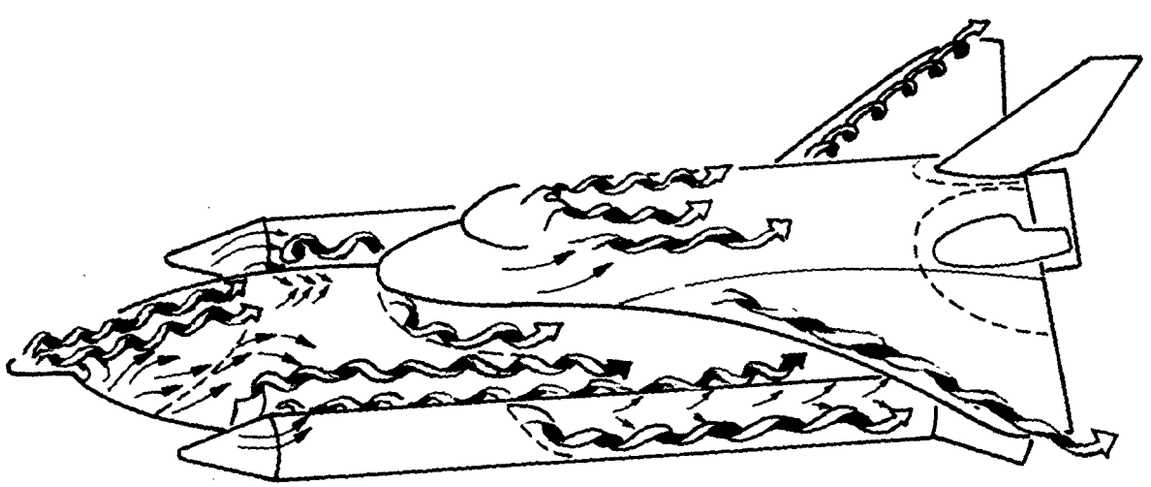

d. FORWARD SRM, M = 1.46

Figure 19. Interference Flow Field (Sheet 2 of 2)

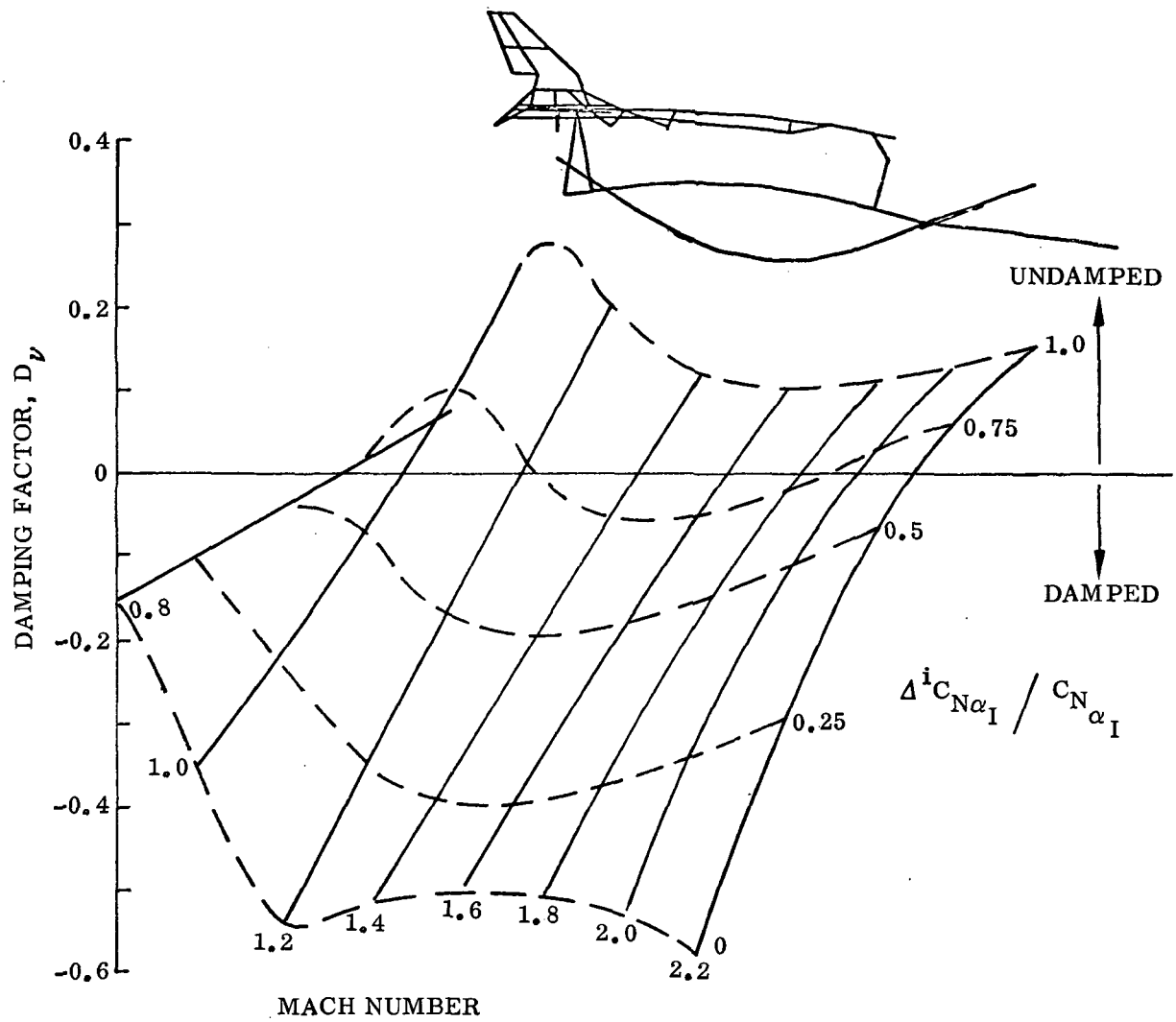

Figure 20. Effect of HO Tank and SRMs on the Aerodynamic Damping Factor of the 049 Booster, 3.64 Hz Symmetric Mode, $\alpha = 0$

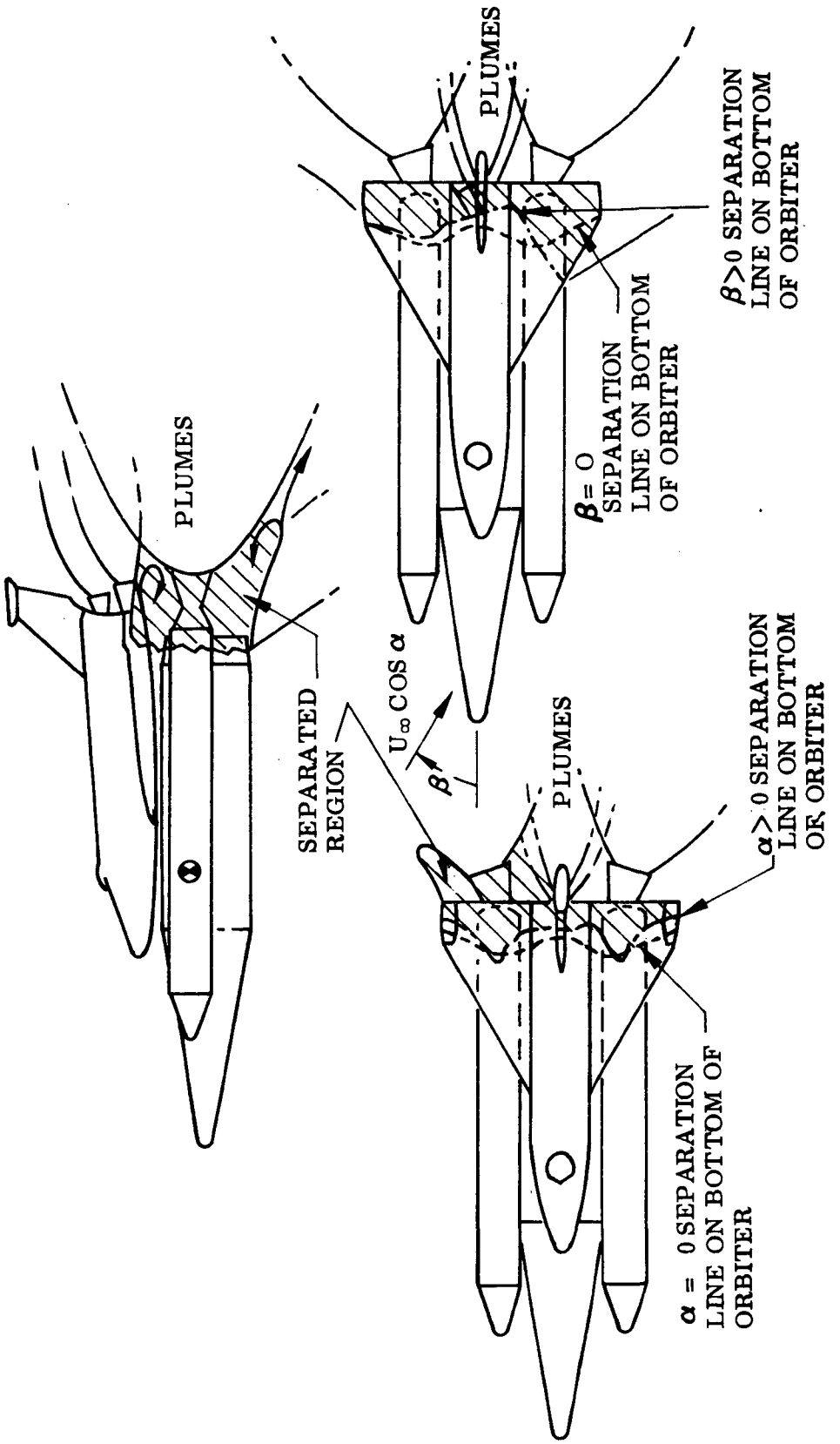

Figure 21. Postulated Effects of Small α and β on Plume-Induced Separation

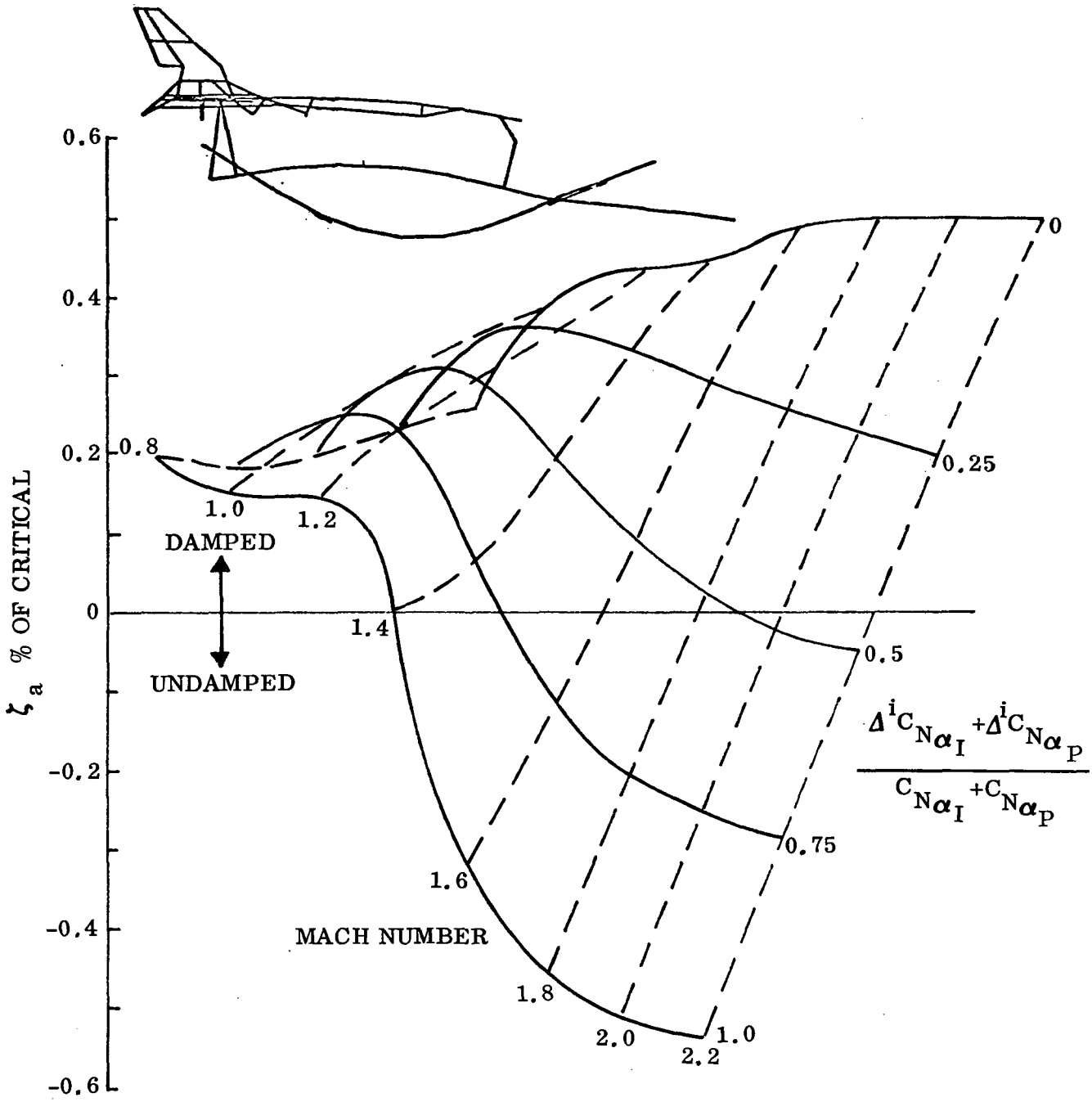

Figure 22. Effect of Solid Plumes and Booster Interference on the Aerodynamic Damping of the 049 Booster, 3.64 Hz Symmetric Mode, $\alpha = 0$

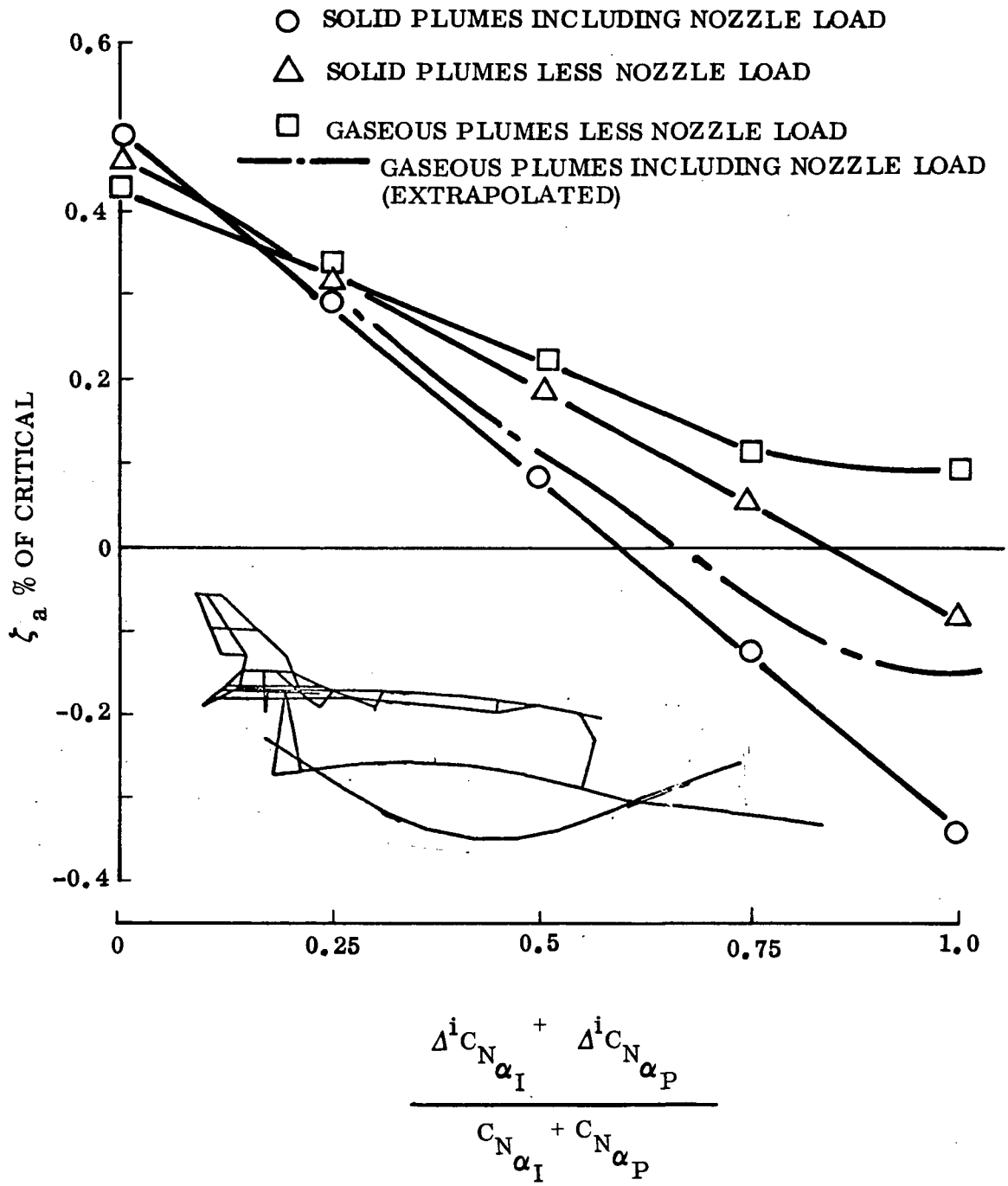

Figure 23. Effect of Gaseous Plumes and Booster Interference on the Aerodynamic Damping of the 049 Booster, 3.64 Hz Symmetric Mode, M = 1.6 and α = 0

Figure 24. Evidence of Leading Edge Vortex-Exhaust Plume Interference on the 049 Booster, M = 1.6, $\alpha = 4^{\circ}$
(Courtesy of Jules Dods, NASA Ames Research Center)

Section 7
CONTROL-INDUCED EFFECTS

An earlier study of the unsteady aerodynamics of a typical phase B orbiter (Refs. 44, 66, and 67) revealed that the vehicle dynamics could be dominated by a number of unsteady flow phenomenon. Essentially three unsteady wing flows were identified which could adversely effect stability. They are:

1. Leeside shock-induced separation
2. Sudden leading edge stall
3. Leading edge vortex burst

The test results for the 040A orbiter show that the critical flow boundaries can be predicted with confidence (Fig. 25). The boundaries of the region of shock-induced flow separation agree quite well with predictions. Likewise, vortex burst is well predicted. Unfortunately, experimental results were not obtained in the region of sudden leading edge stall to test the predictions made from the straight wing data of Ref. 68. However, as the leading edge stall boundary of Ref. 68 comes close to predicting the formation of the leading edge vortex, one would expect that the sudden stall boundaries would also be predicted rather well.

Nonlinear control effects due to coupling between fuselage and wing flow have been measured (Ref. 9 and Fig. 26). These are the results of the shock-induced flow separation forward of the elevon spilling over the forward end of the orbiter maneuvering system (OMS) pod at some critical elevon deflection. Until this spilling occurs, the separation grows linearly with control deflection (δ). At low δ, venting of the separation is restricted at the fuselage-wing juncture by the OMS pod and the separation pocket is vented mainly through its outboard edge near the wing tip. At the critical control deflection, the separation spills over the OMS pod and venting occurs mainly at the wing fuselage juncture (see inset in Fig. 26), causing a skewing of the separation line and inducing sidewash over the tail. This results in nonlinear control

characteristics about all three stability axes (Fig. 26). This "popping" separation is also responsible for the discontinuous yaw characteristics at transonic speeds (Figs. 25 and 27). In this case, it is the sidewash effects on the fuselage boundary layer that causes the discontinuity. Inboard venting occurs for $\beta > 0$, when the left (leeward side) fuselage boundary layer is weak and the separation, as a consequence, is large and spills over the pod. At $\beta \leq 0$, inboard venting is precluded by the OMS pod, as was the case discussed above in connection with Fig. 26 for $\beta = 0$.

There is reason to suspect that the "popping" separation phenomenon discussed above will be associated with hysteresis effects. It is even possible that outright elevon reversal will occur somewhere between $\delta_L = -20^\circ$ and $\delta_L = -40^\circ$; thus, it is desirable to eliminate this flow condition. Of the several means available, moving the pod away from the elevon is probably the simplest. However, the beneficial effects of moving the pod away can be cancelled by increasing the pod size. The orbiter configuration has changed significantly from the 040A (Fig. 28). As the OMS pod was increased in size when it was moved away from the elevon, it is difficult to say whether or not the current configuration will experience a similar undesirable "popping" separation. This must be determined by further experiments.

The prediction of the unsteady flow boundaries for the current configuration (Fig. 29) can be done with a good degree of confidence now, in view of the good correlation of the 040A predictions with experiment (Fig. 25). The current orbiter successfully avoids the region of shock-induced separation over nearly the entire trajectory, except for a relatively quick traverse between M = 2.4 and M = 1.5. However, it takes the orbiter about 90 seconds for even this quick traverse. This gives sufficient time for roll oscillations to grow to a significant magnitude if undamping occurs, as appears possible (Ref. 66). Practically, it is possible that shock-induced separation could occur at a lower angle of attack as a result of leading edge bluntness and fuselage back-pressure effects (Ref. 66). However, for the current α-M trajectory, the duration of the shock-induced separation would not be significantly affected.

The orbiter flies well above the region of shock-induced separation on the strake. Although the upper boundary of this region cannot presently be predicted, Cross (Ref. 69) has shown that for a 75° swept pure delta wing at M = 11, the shock becomes locked to the leading edge at $\alpha = 21°$. For the 80° leading edge sweep of the strake, this occurs at lower α (Ref. 67). Thus, it is very unlikely that the strake will experience shock-induced separation. In fact, one can expect that a leading edge vortex will occur on the strake over the entire Mach number range.

After passing through the region of shock-induced flow separation, the orbiter must negotiate a region of sudden leading edge stall. This boundary was predicted by assuming that the straight wing data of Ref. 68 could be applied to the delta wing when conditions normal to the leading edge are the same. In other words, it was assumed that sudden stall occurred when the angle of attack and Mach number normal to the delta-wing leading edge (α_N and M_N, respectively) corresponded to the sudden stall condition in Ref. 68. $\left[\alpha_N = \tan^{-1}(\tan \alpha / \cos \Lambda) \text{ and } M_N = M_\infty \cos \Lambda (1 + \sin^2 \alpha \tan^2 \Lambda)^{1/2}.\right]$ This may not be entirely true because the spanwise flow component will alter the boundaries just as it did for the occurrence of the leading edge vortex. However, the present orbiter will experience sudden stall, even if it does not occur exactly where predicted. It is likely that the orbiter will have some sideslip and roll when traversing the sudden stall region, especially if it has just experienced roll undamping when traversing the region of shock-induced separation. Thus, sudden stall is likely to occur first on one wing, and snap roll similar to that experienced by the straight wing orbiter (Ref. 70) could result. The strake will not experience sudden stall because the orbiter angle of attack is too high.

Experimental results (Ref. 71) indicate that at low subsonic speeds, the 45° swept wing will probably not develop a leading edge vortex. For the borderline case of a 50° swept delta wing (Ref. 7), the formation of a leading edge vortex is enhanced by a local strong shock at transonic speeds (Ref. 73). Thus, the existence or nonexistence of a leading edge vortex on the 45° swept wing must be determined experimentally. The strake will certainly develop a leading edge vortex at subsonic speeds. The orbiter angle of attack is so high that a leading edge vortex will exist also at supersonic and hypersonic speeds; recent oilflow results verify this (Ref. 8). The strake vortex generates lift on the wing as well as on the strake (Refs. 67, 74). Thus, the orbiter

stability characteristics will be vortex-dependent, and it is desirable to prevent breakdown of the strake vortex on the orbiter wing. Vortex burst is rather unlikely at subsonic speeds as long as the elevon deflection and sideslip angle are small. The data of Ref. 75 show that for a pure 80° delta wing, burst occurs at the orbiter trailing edge at $\alpha = 37.5°$ (Fig. 30). Thus, vortex burst is unlikely to endanger the shuttle flying at $\alpha = 10°$.

Elevon deflection could possibly cause a significant enough change in the subsonic burst attitude to affect the orbiter, especially if the sideslip angle were significant. It has been shown that an obstacle in the wake of a delta wing can induce burst (Ref. 65). An upward elevon deflection (minus δ) can in a similar manner promote vortex burst. This elevon-induced burst will be very sensitive to sideslip (Ref. 76). Current test data (Ref. 9) demonstrate that the spanwise extent of the deflected elevon is a very critical parameter that determines whether or not the burst will cause continuous or discontinuous changes of the aerodynamic characteristics. Because it is planned to trim the shuttle with leeside elevon deflection to minimize control surface heating, this is an area of serious concern. Burst is highly undesirable because it can cause sudden discontinuous changes in pitch, roll, and yaw stability, which often are associated with hysteresis effects (Refs. 66, 67).

Even though the new orbiter differs somewhat from the 040A, it retains the configuration characteristics that are responsible for the discontinuous yaw derivatives; i.e., large leeward elevon deflections, a relatively large fuselage, and large OMS pods. Consequently it is possible that similar effects could occur on the new orbiter. Thus, it appears that the current orbiter will be subject to the same unsteady flow phenomena that plagued earlier configurations, although they will occur during different times in the entry trajectory and their relative seriousness to the vehicle dynamics may be quite different. Further wind tunnel tests are required to supply the experimental data needed to analytically assess the relative seriousness to the vehicle dynamics of the various unsteady flow phenomena.

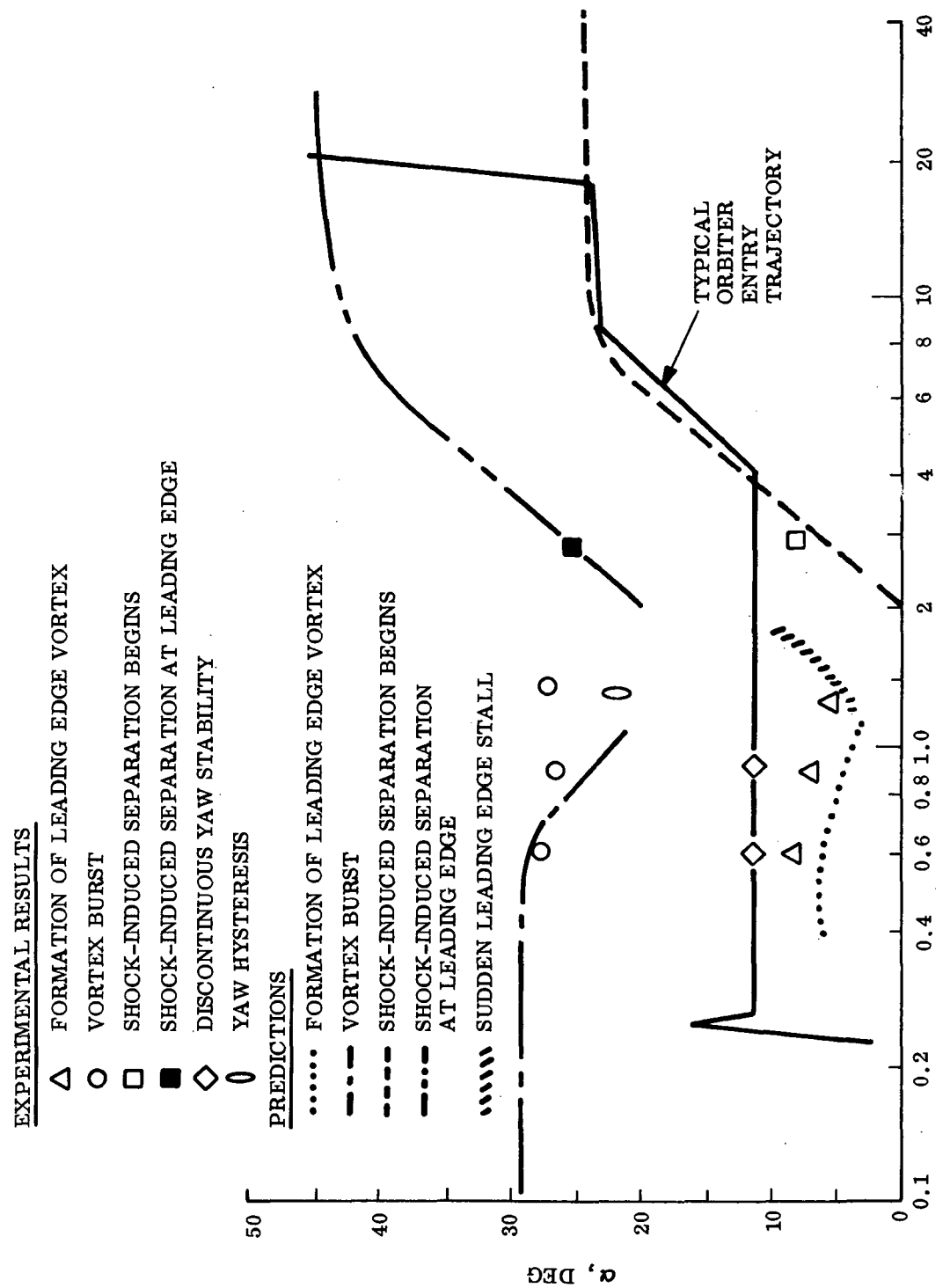

Figure 25. Comparison of Predicted and Measured Unsteady Flow Boundaries for the 040A Orbiter

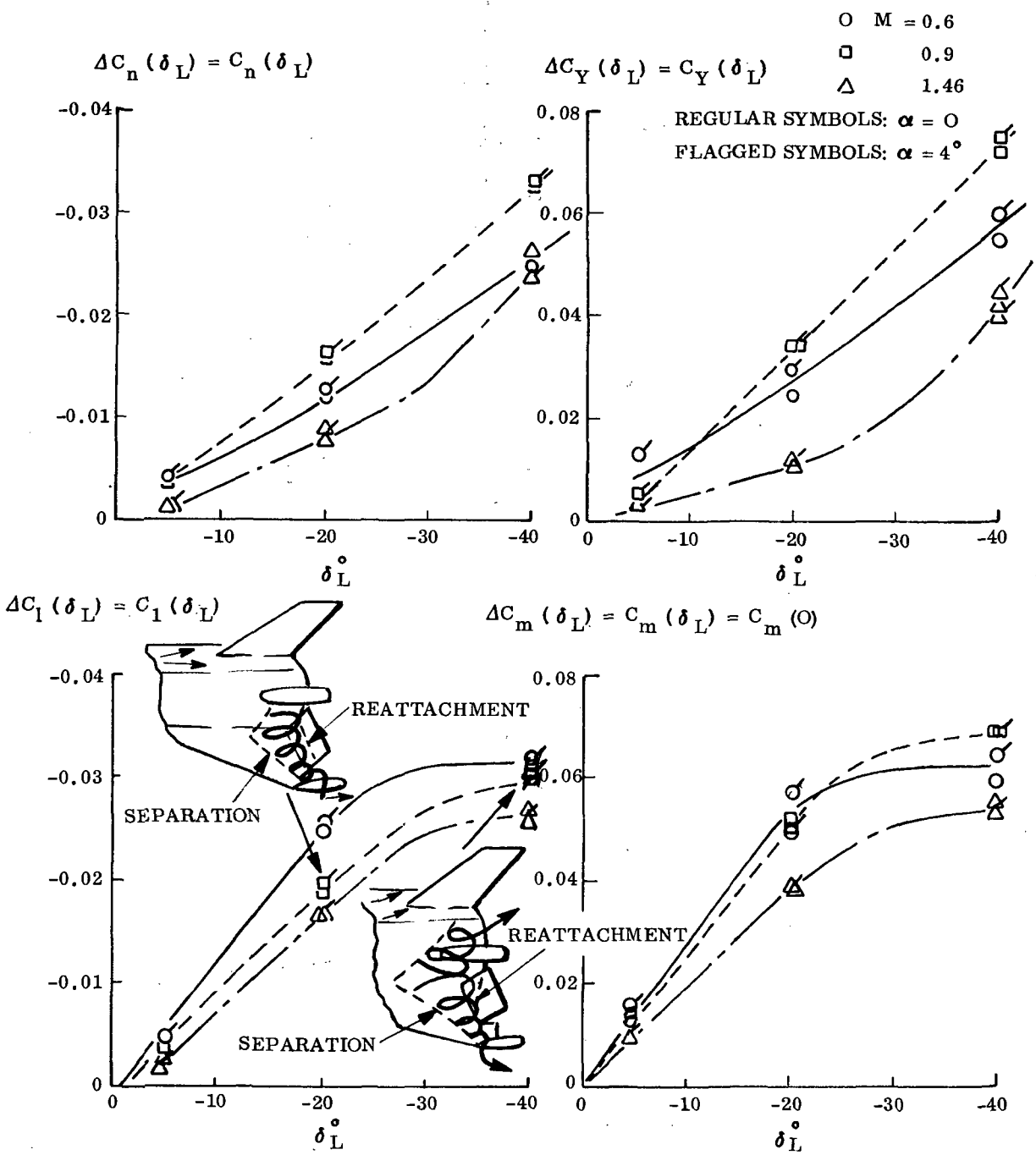

Figure 26. Orbiter Elevon Effectiveness of the 040A Orbiter

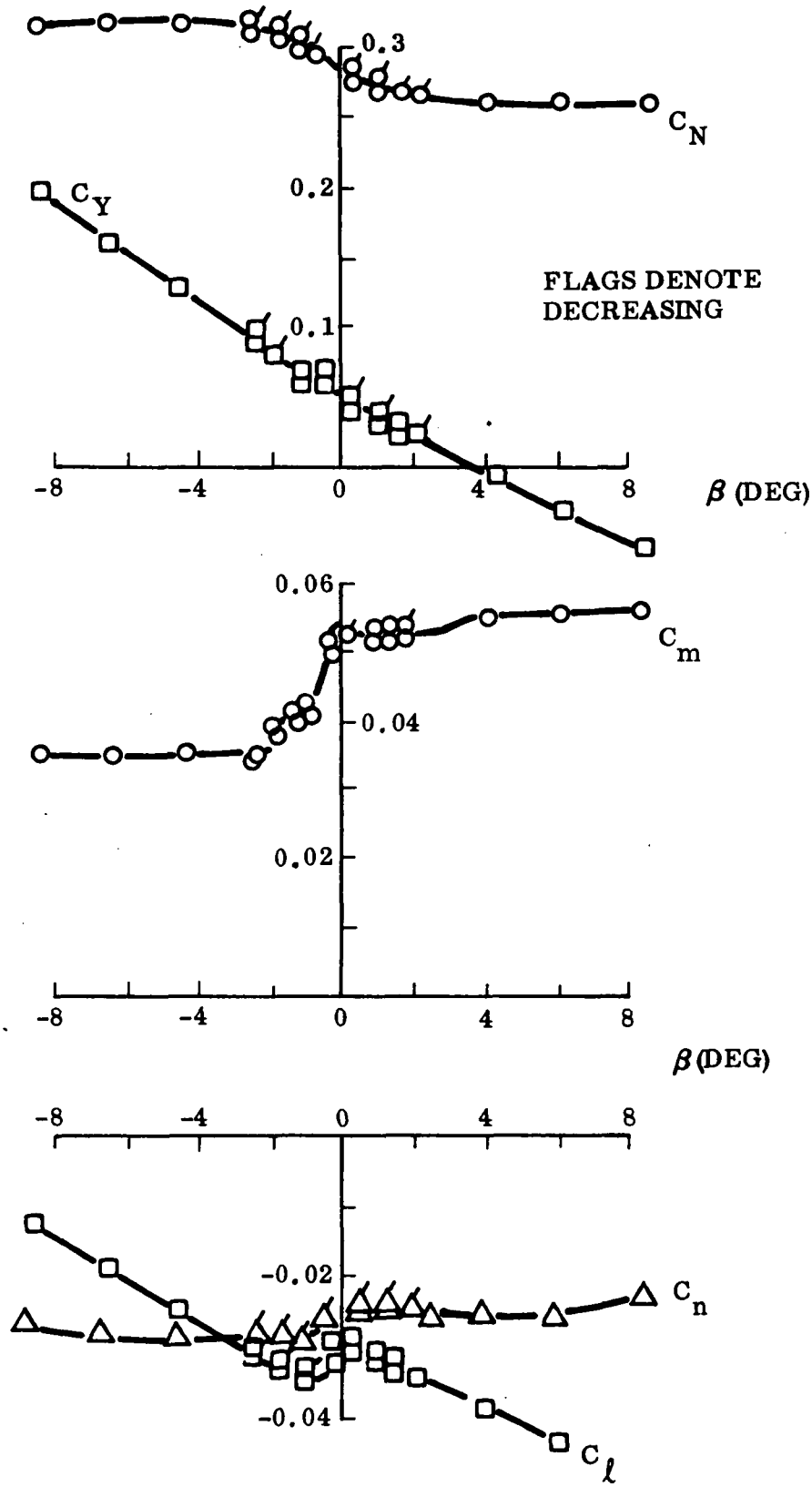

Figure 27. Lateral Stability Characteristics of the 040A Orbiter at M = 0.9 and $\alpha = 11^\circ$

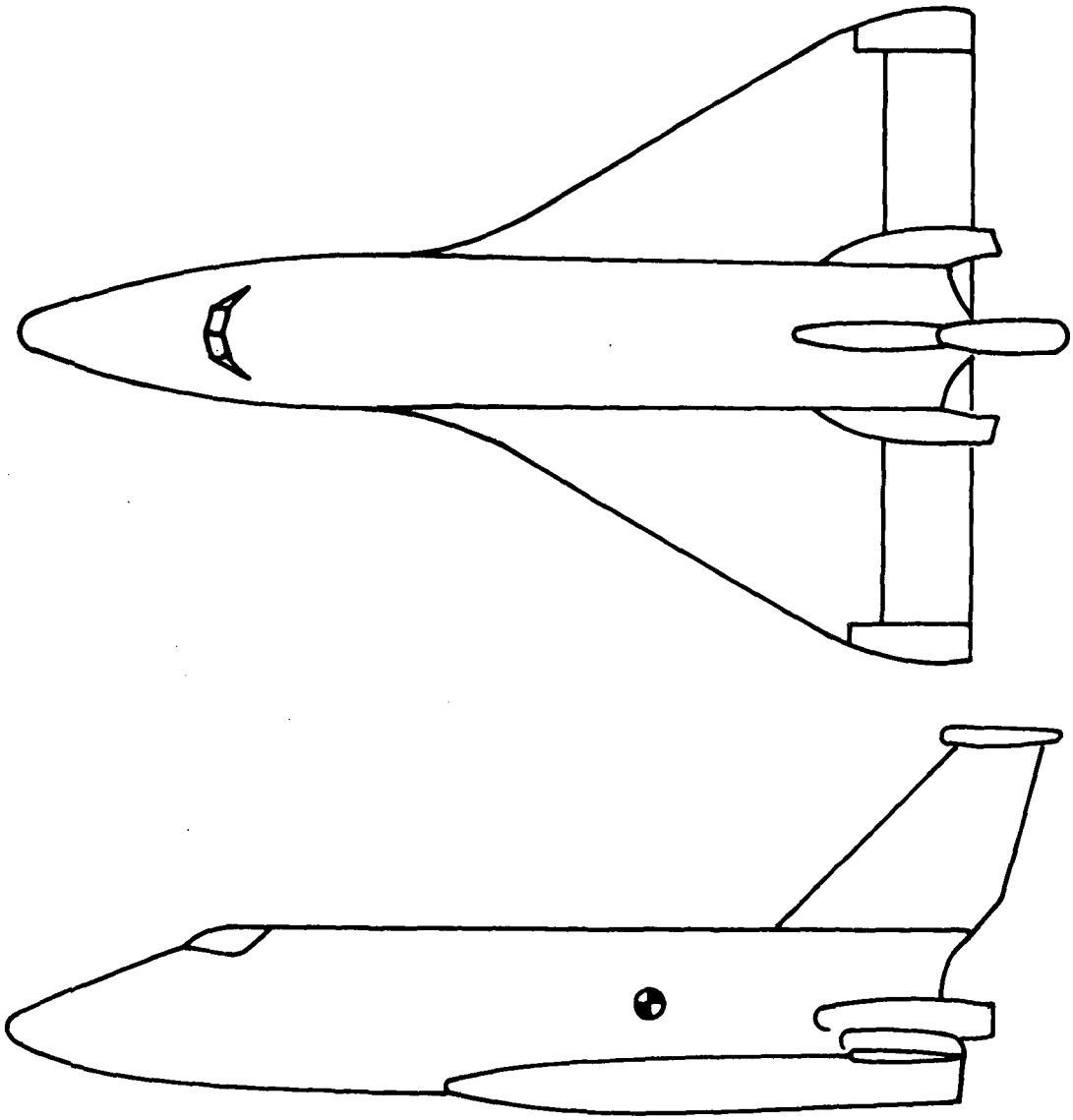

a. 040A ORBITER

Figure 28. Orbiter Configurations (Sheet 1 of 2)

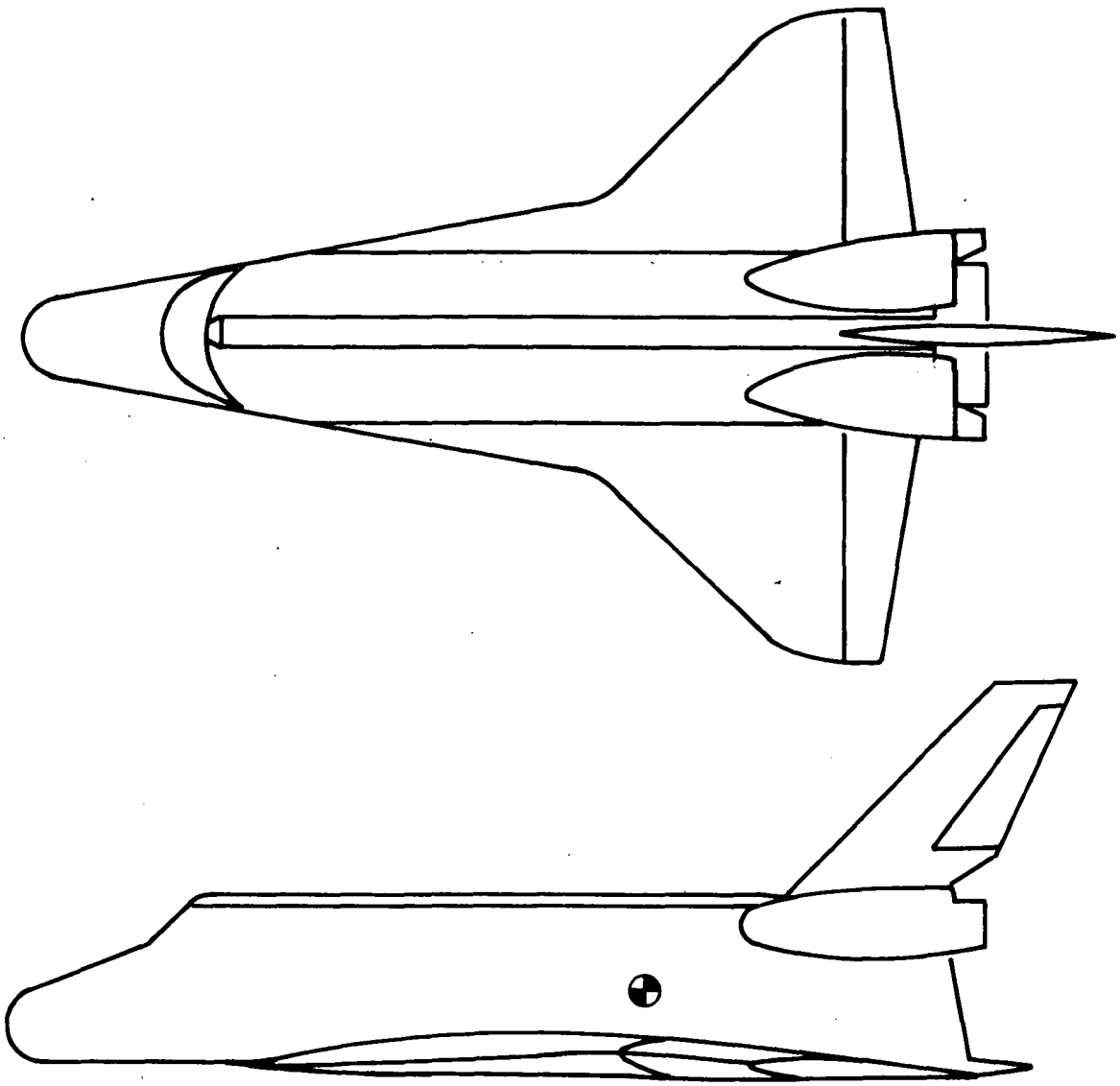

b. CURRENT ORBITER

Figure 28. Orbiter Configurations (Sheet 2 of 2)

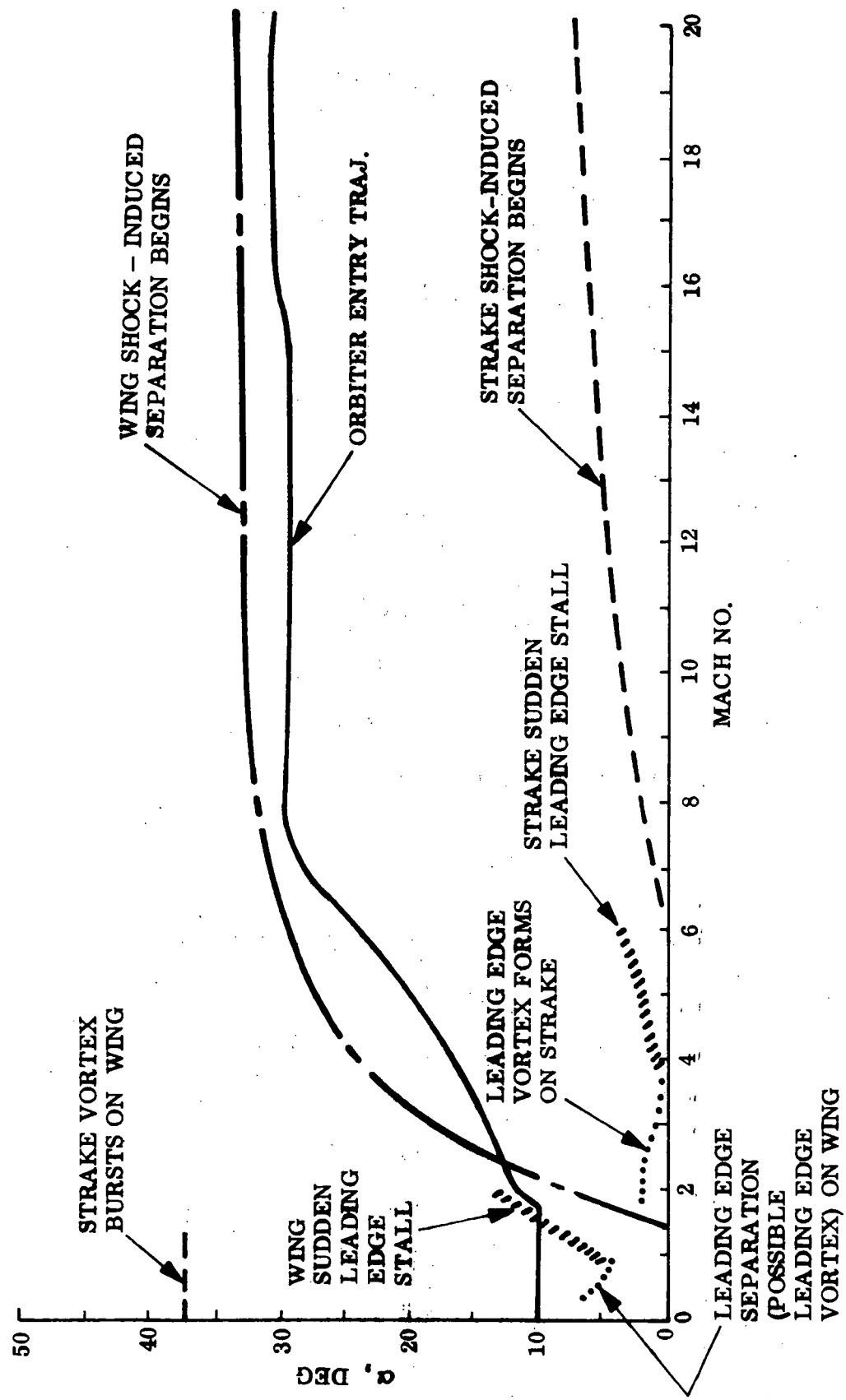

Figure 29. Estimated Unsteady Flow Boundaries for the Current Orbiter

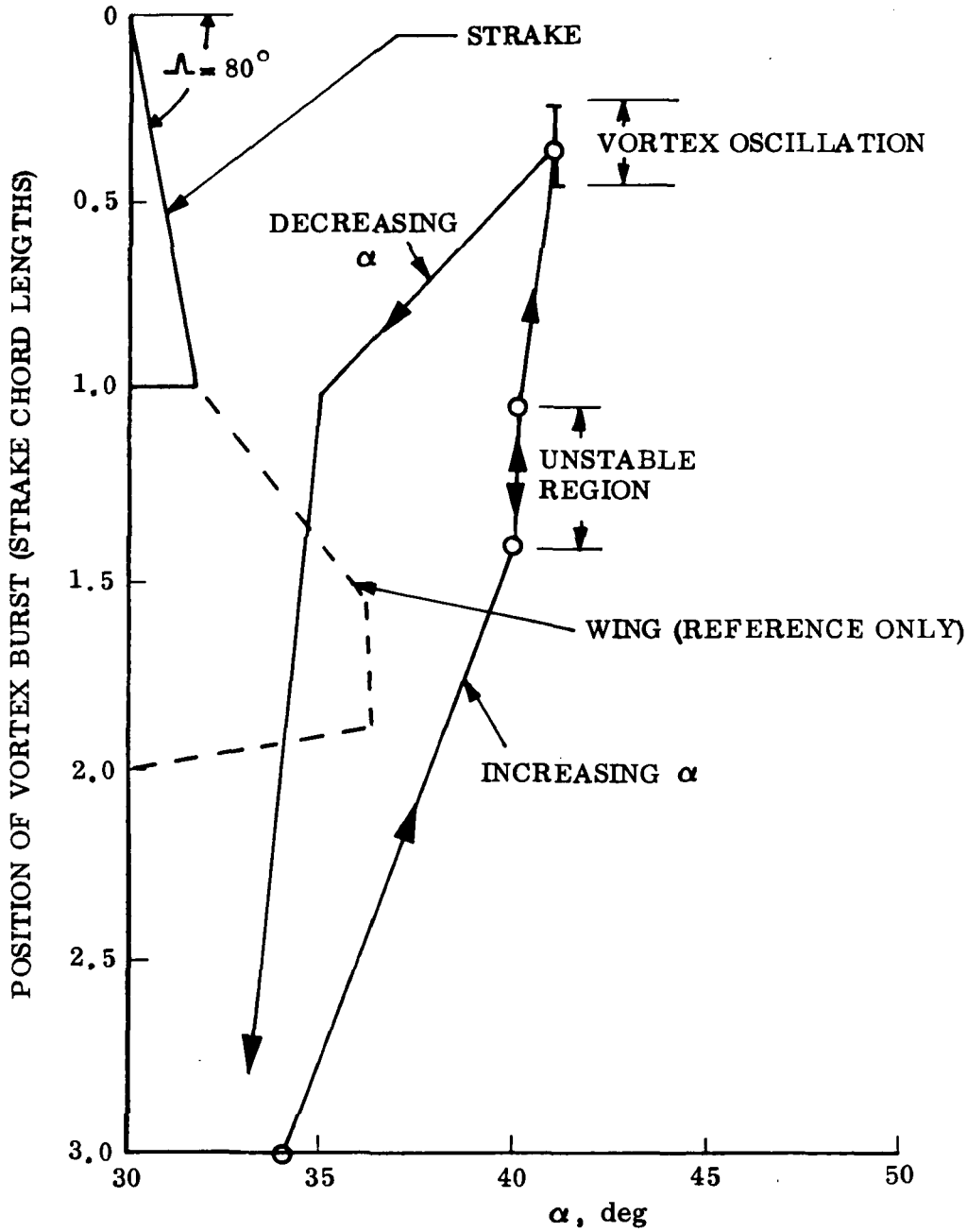

Figure 30. Burst Location and Hysteresis of Strake Vortex at Subsonic Speeds

Section 8
CONCLUSIONS

A study of the unsteady aerodynamics of space shuttle vehicles has shown the following:

- Through a simple modification, Jones' slender wing theory can be applied to give steady and unsteady potential flow characteristics at M = 0. The agreement with experimental data for $\alpha = 0$ is good up to aspect ratios approaching A = 1.5.
- The effects of leading edge vortices on steady and unsteady aerodynamics are determined by a simple analytic theory that currently uses static experimental data to define the longitudinal distribution of vortex-induced loads. Agreement with the limited amount of available experimental data is good for both sharp and rounded leading edges.
- The dominant booster interference results from the rocket exhaust plumes, which induce flow separation on orbiter and booster. Coupling with booster forebody flow field through vortices from separated flow regions provides a mechanism which can possibly cause aeroelastic instability of one or more of the low frequency deformation modes.
- The flow separation induced by the orbiter bow shock also appears likely to cause aerodynamic undamping of the elastic booster. The larger separation on the current configuration and the possible coupling between booster and leeside orbiter flow fields at angle of attack contribute additional possible sources of aerodynamic undamping that should be investigated.
- Elevon control deflections can have large effects on the orbiter flow field, causing nonlinear, often discontinuous changes in the aerodynamic characteristics due to shock-induced flow separation, sudden leading edge stall, vortex burst, and "popping" separation from the OMS pods. The α-M boundaries for the various undesirable, unsteady flow boundaries have been determined using a combined theoretical-experimental approach.

The results of the study indicate that simple analytic tools can be developed to predict the aeroelastic characteristics of the space shuttle ascent configuration.

Section 9
RECOMMENDATIONS FOR FUTURE STUDY

The results of the present study are very encouraging. However, the wide scope of the study has limited the analysis to an exploratory role. More work is clearly needed before the analytic prediction technique for the space shuttle ascent configuration reaches the state of sufficiency accomplished in the past in the prediction of Saturn-Apollo launch vehicles (Refs. 3 through 5). The particular areas in which further work is needed are outlined below without an assignment of priorities.

The unsteady analysis of sharp-edged slender wings is presently semi-empirical and heavily dependent upon a vortex load distribution determined by static experimental data for an A = 1.147 delta wing. The good agreement with static and dynamic experimental data for a wide aspect-ratio range indicates that not only the total vortex lift but also its longitudinal distribution (along the leading edge) is independent of aspect ratio. The empiricism can be removed only after one has learned in quantitative detail why the vortex lift on a delta wing stops growing downstream of some station close to $\xi = 0.4$. The answer to this question could be obtained, it appears, through a study of the experimentally observed effects of the α/θ_{LE} distribution along the leading edge.

To extend the present analysis, with or without the refinement discussed above, to cover the intermediate Mach numbers between M = 0 and M = 1 should not present any great difficulties; and the same is true for the supersonic Mach number range in which subsonic leading edge flow exists.

The simplistic approach taken in the current study to treating the effects of leading edge roundness has to be explored further in spite of, or possibly because of, its apparent success.

Pitch-yaw-roll coupling effects from the leading edge vortices are of special concern for the elastic multi-degree-of-freedom space shuttle ascent configuration. The qualitative results obtained in the current study in regard to vortex-induced effects on lateral unsteady aerodynamics indicate that quantitative prediction is possible. Whether analytic methods can be developed that are not dependent upon static experimental data depends strongly upon the success of resolving the effect of $\alpha/\theta_{LE} = f(\xi)$ on the vortex lift growth, the problem discussed above.

In the current study, analytic tools have been developed for prediction of the unsteady aerodynamics of a slender delta wing describing bending oscillations in the chord-wise plane. The analysis needs to be extended to include more general deformation shapes. Furthermore, the effects of forcing functions due to buffet forces or atmospheric gusts must also be included before a complete analysis of the aeroelastic characteristics of slender (orbiter) wings is possible. The results obtained in the present study indicate that such a complete analytic theory for the elastic slender wing can be developed without destroying the simplicity inherent in the analytic theory presented in this report.

The fact that the present analysis, even though it is rough and rather speculative, predicts negative aerodynamic damping of at least one elastic mode indicates that the problem is of sufficient seriousness to warrant further investigation. It is believed that the analytic tools are essentially in hand to predict the aeroelastic stability of the shuttle booster, provided that the proper static data and a thorough understanding of the flow phenomena are available. The experimental results that will supply the needed input data for such an analysis are outlined briefly below.

First, a consistent set of static experimental data for the correct configuration is required. The bulk of the data required is the usual static aerodynamic data used for design, e.g., pressure distribution results and force data on each body element. To determine which portion of each load component is due to local flow conditions and which portion is due to flow conditions elsewhere, it is recommended that each body element (HO tank, SRM, and orbiter) be pitched and yawed in the presence of the others. This should be done for both pressure distribution and static force tests.

This is a special requirement for the aeroelastic analysis. However, much of the data from the separate perturbation of each body element will also be of use in the analysis of ascent separation dynamics (Ref. 77).

The oilflow results proved invaluable in the present analysis. Likewise, oilflow photographs will be an essential part of any further analysis. Finally, the validity of the analysis can be checked without resorting to very expensive aeroelastic wind tunnel tests by means of special rigid body dynamic tests like those for the Apollo-Saturn boosters (Ref. 78). The response (force, moment, and phase shift) of each body element should be measured while the other elements are oscillated one by one. This will allow the verification of the dynamic effects of the interference loads (Ref. 79).

The present analysis shows that the current orbiter is likely to encounter the following unsteady flow effects:

1. Shock-induced separation on the wing
2. Sudden leading edge stall
3. Elevon-induced burst of the strake vortex
4. Possible elevon-induced discontinuous yaw derivatives.

If any of these effects are judged to be a problem relative to flight dynamics, various courses of action can be taken. The trajectory can be altered to avoid the critical unsteady flow region; the configuration can be altered to eliminate the problem; or the instability may be controlled via stability augmentation. Before a course of action can be chosen, one needs to know the causes of the unsteady flow effects and the extent of the unsteady flow region relative to the entry trajectory for practical variations of α, β, and δ. Also, it is desirable to have a quantitative measure of the effects on both static and dynamic stability derivatives. The following discussion outlines, in principle, a static wind tunnel test program to supply these needed data. The static results can be used in a single-degree-of-freedom dynamic stability analysis (e.g., Ref. 4) to provide a preliminary assessment of the seriousness of the problem. At some later date, special dynamic tests or a more involved analysis will probably be appropriate.

The experimental approach should be similar to but more complete than that reported for the 040A orbiter (Ref. 9). That is, the initial investigation of the unsteady flow region will involve deflection of only one elevon. This allows roll, yaw, and side force data to be used more effectively in gaining a thorough understanding of the phenomena involved. Good quality flow visualization results are vital to an understanding of these complicated, interactive flows. Both oilflow photographs and shadowgraphs should be obtained for all critical flow conditions. Data should also be obtained for realistic deflections of both elevons for certain critical cases. Generally, it may be possible to compute the effects of combined control deflections from data obtained with only one elevon deflected because there is usually very little "cross talk" or coupling between the wing flows. However, when the elevon-induced separation induces body crossflow and alters the leeside vortex trajectories, as frequently happened on the 040A orbiter, strong coupling effects are to be expected.

The recommended test conditions are summarized in Table I. The various unsteady flows are listed in the order in which the entering orbiter will encounter them. These results should reveal the important unsteady flow regions. However, it may be necessary to explore other flight conditions (particularly other Mach numbers) to adequately map the unsteady flow regions. Item 1 concerns strake vortex burst. At hypersonic speeds, the orbiter may encounter burst of the strake vortex even at $\delta = 0$ because of the high angle of attack or upstream effects of the near wake. The wing wake recompression shock has been observed to induce separation on the leeside of a wing at hypersonic speed (Ref. 80). Thus, even when $\delta = 0$, a shock-induced separation will occur on the wing which can affect the vehicle dynamics greatly, if one can judge by similar base recirculation effects on non-lifting re-entry vehicles (Refs. 48 and 81). Items 2 and 3 are straightforward investigations of shock-induced flow separation and sudden stall, respectively. Because discontinuous yaw characteristics could occur throughout the entry trajectory, Item 4 covers the entire Mach number range in the search for these effects. That elevon-induced vortex burst could possibly occur throughout entry is reflected by the test conditions in item 5.

It is possible that shock-induced separation can be converted to sudden stall as the result of elevon back-pressure effects. Furthermore, the change in stall pattern

Table I Summary of Test Conditions

Item	Unsteady Flow Effect	Test Mach	α range	β range	δ range
1	Strake vortex burst	5.0 and 8.0	15° → 35°	0	0
2	Shock-induced separation	1.5 → 3.0	0 → 30°	0	0 → -40°
3	Sudden leading edge stall	0.9 → 2.0	0 → 20°	0	0 → -40°
4	Discontinuous yaw characteristics	8.0	30°	±10°	0 → -40°
		5.0	20°	±10°	0 → -40°
		3.0	15°	±10°	0 → -40°
		2.0	12°	±10°	0 → -40°
		1.5	10°	±10°	0 → -40°
		0.9	10°	±10°	0 → -40°
		0.6	10°	±10°	0 → -40°
		0.3	10°	±10°	0 → -40°
5	Elevon-induced burst of strake vortex	5.0 and 8.0	15° 35°	±10°	0 → -40°
		1.5 → 3.0	0° → 30°	±10°	0 → -40°
		0.3 → 2.0	0° → 20°	±10°	0 → -40°

may persist even after the elevon deflection is reduced below the critical value (Ref. 44). Therefore, it is highly desirable to be able to remotely deflect the elevons to investigate this possible hysteresis. Elevon-induced burst of the strake vortex is likely to exhibit similar hysteresis effects, raising further demands for remote elevon-deflection capability.

An issue of major concern for the proposed test program is the poor Reynolds number scaling that one is forced to accept when trying to simulate the flight conditions of a vehicle as large as the space shuttle. This is a particularly sensitive question where flow separation is concerned because the separation-induced forces (the very forces which one wishes to measure) are known to be very sensitive to Reynolds number effects. Particular care must therefore be taken in the selection and placement of boundary layer trips or distributed roughness. The simulation of the full-scale location of a terminal normal shock (and the associated separated flow region) has been achieved in the wind tunnel by positioning the boundary layer trip so that the boundary layer characteristics at the trailing edge are scaled (Ref. 82). A similar technique could be used for this test. Since a significant separation occurs on the fuselage sides, it will be necessary to scale the boundary layer at the fuselage base as well as at the wing trailing edge. Of special concern is the scaling of the aerodynamics of the free fuselage vortices. It has been found, for instance, that the strong vortex-induced loads that led to spin divergence in the wind tunnel were not realized in flight (Ref. 83). The reason was the poor Reynolds number simulation in the wind tunnel. The boundary layer over the slender nose was laminar in the wind tunnel, with a subcritical separation location in the crossflow plane; whereas the boundary layer was turbulent in flight and the separation was supercritical, which resulted in much weaker asymmetric vortex shedding (Ref. 84). Other examples of similar scaling difficulties appear in Ref. 44. The current orbiter configuration will not experience the same effects of free-body vortices owing to the blunt nose, different α-M history, and the noncircular forebody fuselage cross section. However, the 040A data indicate that body or fuselage vortices can play a significant part in the orbiter aerodynamics, and proper scaling must therefore be ensured.

The occurrence of boundary layer transition and separation on the wing will be affected by the orbiter dynamic motion. Refs. 39 and 37 show that pitch rate affects stall and transition on a wing. This cannot be simulated in a static test and must eventually be investigated analytically or in special dynamic tests.

Recent experimental results (Ref. 85) imply that it may be necessary to simulate the hot orbiter structure in order to obtain correct scaling of the separated flow region. The orbiter will be hot after entry, and the resulting heat transfer to the boundary layer promotes separation. Thus, it is desirable to simulate the wall to free-stream temperature ratio, if possible. This might require heating the model by some means.

At high supersonic and hypersonic speeds the blunt nose on the "current" configuration will generate a curved bow shock with associated entropy gradients in the downstream flow field (Ref. 86). This will affect both the stability and trim characteristics of the orbiter judging by the observed effects on ballistic re-entry vehicles (Ref. 87). There is every reason to expect that the nose bluntness effects for lifting reentry vehicles, such as the space shuttle, will be equally important (Ref. 88). A simple analytic theory already exists for the hypersonic nose bluntness effects on bodies of revolution (Ref. 51). Present work at LMSC under Contract N62269-73-C-0713 will extend this theory to include lifting surfaces as they occur on tactical missiles. The effect of non-hypersonic Mach number, $3 \leq M < 10$, is also to be included. According to preliminary results, the main effect of Mach number is a change of the scaling length (Ref. 89) for the entropy gradient effects, such that the entropy impingement point, i.e., the axial station where the full aft body pressure level is first reached (Ref. 90), moves forward with decreasing Mach number. For a nose bluntness-flow inclination combination such that entropy impingement does not occur upstream of the trailing edge, the orbiter pitching moment would become more stabilizing (more negative) with decreasing Mach number. It would appear that this analysis could readily be extended to geometries typical of the space shuttle orbiter.

Section 10
REFERENCES

1. Runyan, H. L. and Reed, W. H., "Dynamics and Aeroelasticity – An Appraisal," Astronautics & Aeronautics, Vol. 9, No. 2, Feb. 1971, pp. 48–57.

2. Tischler, A. O., "Critical Areas – Thermal-protection Systems, Vehicle Weights, and ---- Aero-elasticity," Astronautics & Aeronautics, Vol. 9, No. 8, Aug. 1971, p. 8.

3. Ericsson, L. E. and Reding, J. P., "Report on Saturn I – Apollo Unsteady Aerodynamics," LMSC-A650215, Feb. 1964, Contract NAS 8-5338, Lockheed Missiles & Space Company, Sunnyvale, Calif.

4. Ericsson, L. E. and Reding, J. P., "Analysis of Flow Separation Effects on the Dynamics of a Large Space Booster," Journal of Spacecraft and Rockets, Vol. 2, No. 4, July–Aug. 1965, pp. 481–490.

5. Ericsson, L. E. and Reding, J. P., "Technical Summary Report, Aeroelastic Characteristics of Saturn 1B and Saturn V Launch Vehicles," LMSC M-37-67-5, Dec. 1967, Contract NAS 8-11238, Lockheed Missiles & Space Company, Sunnyvale, Calif.

6. Hanson, P. W. and Dogget, R. V., Jr., "Wind Tunnel Measurements of Aerodynamic Damping Derivatives of a Launch Vehicle Vibrating in Free-Free Bending Modes at Mach Numbers from 0.7 to 2.87 and Comparisons with Theory," NASA TND 1391, 1962.

7. Ericsson, L. E. and Reding, J. P., "Unsteady Aerodynamic Analysis of Space Shuttle Vehicles, Part II, Steady and Unsteady Aerodynamics of Sharp-Edged Delta Wings," LMSC-D352320, Part II, Aug. 1973, Contract NAS 8-28130, Lockheed Missiles & Space Company, Inc., Sunnyvale, Calif.

8. Reding, J. P. and Ericsson, L. E., "Unsteady Aerodynamic Analysis of Space Shuttle Vehicles, Part III: Booster Interference Effects," LMSC-D352320, Part III, Aug. 1973, Contract NAS 8-28130, Lockheed Missiles & Space Company, Inc., Sunnyvale, Calif.

9. Reding, J. P. and Ericsson, L. E., "Unsteady Aerodynamic Analysis of Space Shuttle Vehicles, Part IV: Effect of Control Deflections on Orbiter Unsteady Aerodynamics," LMSC-D352320, Part IV, Aug. 1973, Contract NAS 8-28130, Lockheed Missiles & Space Company, Inc., Sunnyvale, Calif.

10. Örnberg, T., "A Note on the Flow Around Delta Wings," KTH Aero TN 38, Feb. 1954, Royal Institute of Technology, Stockholm, Sweden.

11. Pick, G. S., "Investigation of Side Forces on Ogive-Cylinder Bodies at High Angles of Attack in the M = 0.5 to 1.1 Range," AIAA 71-570, June 1971.

12. Garner, H. C. and Bryer, D. W., "Experimental Study of Surface Flow and Part-Span Vortex Layers on a Cropped Arrowhead Wing," R&M No. 3107, April 1957, Aeronautical Research Council, Great Britain.

13. Polhamus, E. C., "A Concept of the Vortex Lift of Sharp-Edge Delta Wings Based on a Leading-Edge-Suction Analogy," NASA TN D-3767, Dec. 1966.

14. Polhamus, E. C., "Predictions of Vortex-Lift Characteristics by a Leading-Edge Suction Analogy," Journal of Aircraft, Vol. 8, No. 4, April 1971, pp. 193–199.

15. Jones, R. T., "Properties of Low-Aspect-Ratio Pointed Wings at Speeds Below and Above the Speed of Sound," NASA Report No. 835, May 1945.

16. Peckham, O. H., "Low-Speed Wind-Tunnel Tests on a Series of Uncambered Slender Pointed Wings with Sharp Edges," R&M No. 3186, Dec. 1958, Aeronautical Research Council, Great Britain.

17. Earnshaw, P. B. and Lawford, J. A., "Low-Speed Wind-Tunnel Experiments on a Series of Sharp-Edged Delta Wings: Part 1. Forces, Moments, Normal-Force Fluctuations, and Positions of Vortex Breakdown," Tech. Note AERO 2780, Aug. 1961, Aeronautical Research Council, Great Britain.

18. Fink, P. T., "Some Low Speed Experiments with 20 Degree Delta Wings," Zeitschrift für Flugwissenschaften, Vol. 4, No. 7, July 1956, pp. 247–249.

19. Lawford, J. A. and Beauchamp, A. R., "Low-Speed Wind-Tunnel Measurements on a Thin Sharp-Edged Delta Wing with 70° Leading-Edge Sweep, with Particular Reference to the Position of Leading-Edge-Vortex Breakdown," R&M No. 3338, Nov. 1961, Aeronautical Research Council, Great Britain.

20. Tosti, L. P., "Low-Speed Static Stability and Damping-in-Roll Characteristics of Some Swept and Unswept Low-Aspect-Ratio Wings," NASA TN 1468, 1947.

21. Bartlett, G. E. and Vidal, R. J., "Experimental Investigation of Influence of Edge Shape on the Aerodynamic Characteristics of Low Aspect Ratio Wings at Low Speeds," Journal of the Aeronautical Sciences, Vol. 22, No. 8, Aug. 1955, pp. 517–533.

22. Davenport, E. E. and Huffman, J. K., "Experimental and Analytical Investigation of Subsonic Longitudinal and Lateral Aerodynamic Characteristics of Slender Sharp-Edge 74° Swept Wings," NASA TND-6344, July 1971.

23. Wentz, W. H. Jr., "Effects of Leading-Edge Camber on Low Speed Characteristics of Slender Delta Wings," NASA CR-2002, 1972.

24. Snyder, M. J. Jr. and Lamar, J. E., "Application of the Leading-Edge Suction Analogy to Prediction of Longitudinal Load Distribution and Pitching Moments for Sharp-Edged Delta Wings," NASA TND 6994, Aug. 1972.

25. Bisplinghoff, R. L., Ashley, H., and Halfman, R. L., Aeroelasticity, Addison-Wesley, Cambridge, Mass., 1955, pp. 418–419.

26. Woodcock, D. L., "A Comparison of Methods Used in Lifting Surface Theory," AGARD Report No. 583, June 1971.

27. Lambourne, N. C., Bryer, D. W., and Maybrey, J. F. M., "The Behavior of the Leading-Edge Vortices over a Delta Wing Following a Sudden Change of Incidence," R&M No. 3645, March 1969, Aeronautical Research Council, Great Britain.

28. Lambourne, N. C., Bryer, D. W., and Maybrey, J. F. M., "Pressure Measurements on a Model Delta Wing Undergoing Oscillatory Deformation," NPL Aero Report 1314, March 1970, Aeronautical Research Council, Great Britain.

29. Woodgate, L., "Measurements of the Oscillatory Pitching Moment Derivatives on a Slender Sharp-Edged Delta Wing in Incompressible Flow," R&M No. 3628, Part 2, July 1968, Aeronautical Research Council, Great Britain.

30. Woodgate, L. and Pugh, P. G., "Measurements of the Pitching-Moment Derivatives on a Sharp-Edged Delta Wing in Incompressible Flow," R&M No. 3379, 1963.

31. Woodgate, L. and Halliday, A. S., "Measurements of Lift, Drag, and Pitching Moments on a Series of Three Delta Wings," R&M No. 3628, Part 4, July 1968, Aeronautical Research Council, Great Britain.

32. Gersten, K., "Nichtlineare Tragflächen Theorie insbesondere für Tragflügel mit kleinen Seitenverhältnis," Ingenieur-Archiv, Vol. 30, 1961, pp. 431–452.

33. Ville, G., "Influence des Decallements au Bord d'Attaque sur les Characteristiques Aerodynamiques des Voilures," Association Francaise des Ingenieurs et Techniciens des l'Aeronautique et de l'Espace, Colloque d'Aerodynamique Appliquée, 4th, Lille, France, Nov. 8–10, 1967.

34. Woodgate, L., "Measurements of the Oscillatory Pitching Moment Derivatives on a Delta Wing with Round Leading Edges in Incompressible Flow," R&M No. 3628, Part 1, July 1968, Aeronautical Research Council, Great Britain.

35. Woods, P. and Ericsson, L. E., "Aeroelastic Considerations in a Slender, Blunt-Nose, Multistage Rocket," Aerospace Engineering, Vol. 21, No. 5, May 1962, pp. 42–51.

36. Ericsson, L. E., "Aeroelastic Instability Caused by Slender Payloads," J. Spacecraft and Rockets, Vol. 4, No. 1, Jan. 1967, pp. 65–73.

37. Ericsson, L. E., "Effects of Boundary Layer Transition on Vehicle Dynamics," J. Spacecraft and Rockets, Vol. 6, No. 12, pp. 1404-1409, December 1969.

38. Ericsson, L. E. and Reding, J. P., "Unsteady Airfoil Stall," NASA CR 66787, July 1969.

39. Ericsson, L. E. and Reding, J. P., "Unsteady Airfoil Stall and Stall Flutter," NASA CR 111906, July 1971.

40. Larson, P. O., "A Note on Supersonic and Transonic Flow Around Delta Wings," Seminar on Wind-Tunnel Techniques and Aerodynamics, Royal Institute of Technology, Stockholm, May 1954.

41. Squire, L. C., Jones, J. G., and Stanbrook, A., "An Experimental Investigation of Some Plane and Cambered 65° Delta Wings at Mach Numbers from 0.7 to 2.0," R&M No. 3305, July 1961, Aeronautical Research Council, Great Britain.

42. Stanbrook, A. and Squire, L. C., "Possible Types of Flow at Swept Leading Edges," Aeronautical Quarterly, Feb. 1964, pp. 72–82.

43. Rogers, E. W. E., "A Study of the Effect of Leading-Edge Modification on the Flow over a 50° Sweptback Wing at Transonic Speeds," R&M 3270, 1970, Aeronautical Research Council, Great Britain.

44. Reding, J. P. and Ericsson, L. E., "Review of Delta Wing Space Shuttle Vehicle Dynamics," Final Technical Report, LMSC-D243938, Oct. 1971, Contract NAS 9-11495, Lockheed Missiles & Space Company, Inc., Sunnyvale, Calif.

45. Ericsson, L. E., "Loads Induced by Terminal-Shock Boundary-Layer Interaction on Cone-Cylinder Bodies," Journal of Spacecraft and Rockets, Vol. 7, No. 9, Sept. 1970, pp. 1106–1112.

46. Ericsson, L. E., "Unsteady Aerodynamics of Separating and Reattaching Flow on Bodies of Revolution," Recent Research on Unsteady Boundary Layers, Vol. 1, IUTAM Symposium, Laval University, Quebec, 24–28 May 1971, pp. 481–512.

47. Ericsson, L. E. and Reding, J. P., "Dynamics of Separated Flow Over Blunt Bodies," Technical Summary Report, LMSC 2-80-65-1, Dec. 1965, Contract NAS 8-5338, Lockheed Missiles & Space Company, Sunnyvale, Calif.

48. Ericsson, L. E. and Reding, J. P., "Re-Entry Capsule Dynamics," Journal of Spacecraft and Rockets, Vol. 8, No. 6, June 1971, pp. 575–586.

49. Brown, C. E., "Theoretical Lift and Drag of Thin Triangular Wings at Supersonic Speeds," NACA Report No. 839, Nov. 1946.

50. Hayes, W. D. and Probstein, R. F., Hypersonic Flow Theory, New York and London, 1959.

51. Ericsson, L. E., "Unsteady Embedded Newtonian Flow," Astronautica Acta, 1973.

52. Ericsson, L. E., Reding, J. P. and Guenther, R. A., "Launch Vehicle Gust Penetration Loads," Journal of Spacecraft and Rockets, Vol. 9, No. 1, Jan. 1973, pp. 19–25.

53. Ericsson, L. E., Reding, J. P., and Guenther, R. A., "Elastic Launch Vehicle Response to Sinusoidal Gusts," Journal of Spacecraft and Rockets, Vol. 10, No. 5, May 1973, pp. 244–252.

54. Ericsson, L. E., "Dynamic Effects of Shock-Induced Flow Separation," AIAA 73-308, March 1973.

55. Lott, R. A. and Ramsey, P., "An Investigation of the Load Distribution over the SRB and External Tank of a 0.004 Scale Model of the 049 Space Shuttle Launch Configuration," NASA CR 120, 058, March 1973.

56. Treon, S. L., "Effects of Nose-Cone Angle on the Transonic Aerodynamic Characteristics of a Blunt Cone-Cylinder Body Having a Cylindrical, Flared, or Blunt-Finned Afterbody," NASA TM X-582, October 1961.

57. Edney, B. E., "Effects of Shock Impingement on the Heat Transfer around Blunt Bodies," AIAA Journal, Vol. 6, No. 1, June 1968, pp. 15–23.

58. Reding, J. P., French, N. J., Jecmen, D. M., and Ericsson, L. E., "The Aeroelastic Characteristics of the Saturn IB and Saturn V Launch Vehicles," M-37-65-1, Lockheed Missiles & Space Company, Inc., March 1965.

59. Kuehn, Donald M., "Turbulent Boundary-Layer Separation Induced by Flares on Cylinders at Zero Angle of Attack," NASA TR-117, 1961.

60. Brownson, J. J., Whitnah, A. M., Kassner, D. L., and Rampy, J., "Aerodynamic Characteristics of an 040A Space Shuttle Configuration with Simulated Rocket Plumes at Mach Numbers from 0.8 to 2.2," NASA TMX-62, 126 (SSPD-88) Sept 1972.

61. Dods, J. B. Jr., Brownson, J. J., Blackwell, K. L., Decker, J. P., Kassner, D. L., and Roberts, B. B., "Effect of Gaseous and Solid Simulated Rocket Plumes on an 040A Space Shuttle Configuration at Mach Numbers from 1.6 to 2.2," Prospective NASA TM.

62. Henderson, A. Jr., "Aerothermodynamic Technology for Space Shuttle – and Beyond," AIAA Paper 73-59, presented at the AIAA 9th Annual Meeting and Technical Display, January 1973.

63. Low, P. F. and Stuhlman, C. E., "Lift-off Vibration Characteristics MSC Model 049 Shuttle Configuration," Northrop Services, Inc., internal document 9243D-72-11, 16 August 1972.

64. Anon., "Aerodynamic Design Data Book, Vol. I," North American Rockwell Report SD72-SH-60-1, 1972.

65. Hummel, D., "Untersuchungen über das Aufplatzen der Wirbel an schlanken Deltaflügeln," Zeitschrift für Flugwissenschaften 13, 1965, pp. 158–168.

66. Reding, J. P. and Ericsson, L. E., "Effects of Delta Wing Separation on Shuttle Dynamics," Journal of Spacecraft and Rockets, Vol. 10, No. 7, July 1973, pp. 421–428.

67. Reding, J. P. and Ericsson, L. E., "Review of Delta Wing Space Shuttle Vehicle Dynamics," Vol. III, Proceedings Space Shuttle Aerothermodynamics Conference, NASA Ames RC, Moffett Field, Calif, Dec. 15–16, 1971, NASA TMX-2508, pp. 861–931.

68. Lindsey, W. F. and Landrum, E. J., "Compilation of Information on the Transonic Attachment of Flows at the Leading Edges of Airfoils," NACA TN 4204, Feb. 1958.

69. Cross, E. J., "Analytical Investigation of the Expansion Flow Field over a Delta Wing at Hypersonic Speeds," ARL 68-0027, Feb. 1968.

70. Hamilton, E. J. and Ryals, W. G., "Review of 1/10 Scale Shuttle Air Drop Test Results," MSC Internal Document 5-2950-1-HOU-126, June 1970, NASA.

71. Graham, D., "The Low-Speed Lift and Drag Characteristics of a Series of Airplane Models Having Triangular or Modified Triangular Wings," NACA RM A53D14, June 15, 1953.

72. Wentz, W. H. Jr., and Kohlman, D. L., "Vortex Breakdown on Sharp-Edged Wings," AIAA Paper No. 69-778, July 1969.

73. Mullons, E. and Linsley, C. E., "Buffet Dynamic Loads during Transonic Maneuvers," AFFDL-TR-72-46, September 1972, Air Force Flight Dynamic Lab., Wright-Patterson Air Force Base, Ohio.

74. Wentz, W. H. Jr., and McMahon, M. C., "Further Experimental Investigations of Delta and Double-Delta Wing Flow Fields at Low Speeds," NASA CR-714, February 1967.

75. Lowson, M. V., "Some Experiments with Vortex Breakdown," Journal of the Royal Aeronautical Society, Vol. 68, May 1964, pp. 343–346.

76. Hummel, D., "Experimentelle Unterschung der Strömung auf der Saugseite eines Schlanken Deltaflügels," Zeitschrift für Flugwissenschaften, Vol. 13, No. 7, July 1965, pp. 247–252.

77. Orlik-Rückeman, K. J., LaBerge, J. G., and Hanff, E. S., "Experiments on the Dynamic Stability of the Space Shuttle," Space Shuttle Aerothermodynamics Technology Conference, Volume III, Aerodynamics, NASA TM X-2508, Dec. 15–16, 1971.

78. Reding, J. P., "Partial Simulation of Elastic-Body Dynamics for the Upper-Stage Apollo-Saturn Launch Vehicle," LMSC M-37-67-4, Lockheed Missiles & Space Co. Inc., Sunnyvale, Calif., Dec. 1967.

79. Orlik-Rückeman, K. J., "Survey of Needs and Capabilities for Wing Tunnel Testing of Dynamic Stability of Aircraft at High Angles of Attack," NASA CR-114583, 1973.

80. Hulcher, G. D. and Behrens, W., "Viscous Hypersonic Flow over a Flat Plate at Angle of Attack with Leeside Boundary Layer Separation," Proceedings of the 1972 Heat Transfer and Fluid Mechanics Institute, Northridge, Calif., June 1972.

81. Ericsson, L. E. and Reding, J. P., "Aerodynamic Effects of Bulbous Bases," NASA CR 1339, August 1969.

82. Blackwell, J. A. Jr., "Preliminary Study of Effects of Reynolds Number and Boundary-Layer Transition Location on Shock-Induced Separation," NASA TN D-5003, January 1969.

83. Anderson, C. A., "Stall/Post-Stall Characteristics of the F-111 Aircraft," Paper No. 18, AGARD Specialists' Meeting on Fluid Dynamics of Aircraft Stalling, Lisbon, Portugal, April 26–28, 1972.

84. Ericsson, L. E., "Report on Visit to the AGARD Specialists' Meeting on the Fluid Dynamics of Aircraft Stalling, Lisbon, Portugal, April 26–28, 1972," LMSC-TIC-2061, 6 Sept. 1972.

85. Macha, J. M., Norton, D. J., and Young, J. C., "Surface Temperature Effects on Subsonic Stall," AIAA Paper No. 72-960, Sept. 1972.

86. Ericsson, L. E., "Unsteady Aerodynamics of an Ablating Flared Body of Revolution Including Effects of Entropy Gradient," AIAA Journal, Vol. 6, No. 12, Dec. 1968, pp. 2395–2401.

87. Ericsson, L. E., "Effect of Nose Bluntness, Angle of Attack, and Oscillation Amplitude on Hypersonic Unsteady Aerodynamics of Slender Cones," AIAA Journal, Vol. 9, No. 2, Feb. 1961, pp. 297–304.

88. Ericsson, L. E. and Reding, J. P., "Dynamic Stability Problems Associated with Flare Stabilizers and Flap Controls," Journal of Spacecraft and Rockets, Vol. 7, No. 2, Feb. 1970, pp. 132–137.

89. Ericsson, L. E., "Universal Scaling Laws for Hypersonic Nose Bluntness Effects," AIAA Journal, Vol. 7, No. 12, Dec. 1969, pp. 2222–2227.

90. Ericsson, L. E., "Transition Effects on Slender Vehicle Stability and Trim Characteristics," Paper 73-126, AIAA 11th Aerospace Sciences Meeting, Washington, D.C., Jan. 10–12, 1973.

Appendix A
NOMENCLATURE

A	aspect ratio, $A = b^2/S$
b	wing span
$\bar{c}$	reference length, usually mean aerodynamic chord: $\bar{c} = 2\ c_o/3$ for a delta wing
c_o	slender wing root chord
D_ν	elastic vehicle damping
L	lift: coefficient $C_L = L/(\rho_\infty\ U_\infty^2/2)S$
ℓ	rolling moment: coefficient $C_\ell = \ell/(\rho_\infty\ U_\infty^2/2)Sb$
M	Mach number
M_p	pitching moment: coefficient $C_m = M_p/(\rho_\infty\ U_\infty^2/2)S\bar{c}$
N	normal force: coefficient $C_N = N/(\rho_\infty\ U_\infty^2/2)S$
n	yawing moment: coefficient $C_n = n/(\rho_\infty\ U_\infty^2/2)Sb$
p	static pressure: coefficient $C_p = (p - p_\infty)/(\rho_\infty\ U_\infty^2/2)$
q	pitch rate
Re	Reynolds number based on c_o and free stream conditions
S	reference area
U	velocity
x	axial body-fixed coordinate (x = 0 at wing apex)
Y	side force: coefficient $C_Y = Y/(\rho_\infty\ U_\infty^2/2)S$
α	angle of attack

α_o	trim angle of attack
β	side slip angle
δ	control deflection
ϵ	vortex contribution to apparent mass
ζ	structural damping, fraction of critical damping
ζ_a	aerodynamic damping, fraction of critical damping
θ	angular perturbation
θ_{LE}	apex half angle
θ_{TE}	trailing edge sweep angle
Λ	leading edge sweep angle, $\Lambda = \pi/2 - \theta_{LE}$
ξ	dimensionless x-coordinate, $\xi = x/c_o$
ρ	air density
ω	free-free bending frequency and rigid body pitching frequency
$\overline{\omega}$	reduced frequency, $\overline{\omega} = \omega c_o/U_\infty$

Subscripts

CG	center of gravity
I	interference flow field
L	left elevon
LE	leading edge
N	normal to leading edge
ν	harmonic component
P	plume
R	right elevon
TE	trailing edge
∞	free stream conditions

Superscripts

(i) induced, e.g., $\Delta^{i}C_{N}$ = normal force component not dependent upon local flow conditions

Differential Symbols

$\dot{\theta} = \partial\theta/\partial t$; $\ddot{\theta} = \partial^2\theta/\partial t^2$

$C_{L_\alpha} = \partial C_L/\partial\alpha$; $C_{\ell_\beta} = \partial C_\ell/\partial\beta$; $C_{m_\theta} = \partial C_m/\partial\theta$

$C_{m_{\dot{\theta}}} = C_{m_q} + C_{m_{\dot{\alpha}}} = \partial C_m/\partial\,(\bar{c}\,\dot{\theta}/U_\infty)$; $C_{mq} = \partial C_m/\partial\,(\bar{c}q/U_\infty)$